Simulated Signatures of Greenland Melting in the North Atlantic: A Model Comparison With Argo Floats, Satellite Observations, and Ocean Reanalysis

Sophie Stolzenberger[1] , **Roelof Rietbroek[2], Claudia Wekerle[3]** , **Bernd Uebbing[1]** , and **Jürgen Kusche[1]**

[1]Institute of Geodesy and Geoinformation, University of Bonn, Bonn, Germany, [2]ITC-WRS, Faculty of Geo-information Science and Earth Observation, University of Twente, Enschede, The Netherlands, [3]Alfred Wegener Institute Helmholtz Center for Polar and Marine Research (AWI), Bremerhaven, Germany

Abstract Increased Greenland ice sheet melting has an impact on global mean and regional sea level rise and the ocean circulation. In this study, we explore whether Greenland melting signatures found in ocean model simulations are visible in observations from radar altimetry, satellite gravimetry and Argo floats. We have included Greenland freshwater flux (GF) in the global Finite-Element-Sea ice-Ocean Model (FESOM) for the years 1993–2016. The reference run is computed by excluding Greenland freshwater input. These experiments are performed on a low resolution (ca. 24 km) and a high resolution (ca. 6 km) eddy-permitting mesh. For comparison with the model experiments, we use different observational data, such as Argo floats, satellite observations, and reanalyses. We find that surface GF maps into signatures in temperature and salinity down to about 100 m in the surroundings of Greenland. The simulated melting signatures are particularly visible in steric heights in Baffin Bay and Davis Strait. Here, we find an improvement of the mean square error of up to 30% when including GF. For the Nordic part of the Nordic Seas, however, we find no improvement when including GF. We compare steric heights with reanalysis data and a new setup of the inversion method from gravimetric and altimetric satellite data. We cannot confirm that the GF signatures on variables such as temperature and salinity are visible in the observations on the time scales considered. However, we find that increased model resolution often causes larger improvements than occur due to including the simulated melting effect.

Plain Language Summary In recent years, Greenland's freshwater contribution to the ocean has increased due to the accelerated melting of its ice sheet and glaciers. In this study, we investigate the importance of this melting in reproducing the observed characteristics of the northern part of the North Atlantic Ocean in a numerical ocean model. To do that, we compare the results of two model simulations, one with and one without Greenland melt, with in situ observations or data from satellites. The inclusion of Greenland melt results in a better model representation of the ocean in terms of salinity, temperature, and sea level anomalies, especially in Baffin Bay on the west side of Greenland. We also discuss the role of a higher model resolution on the simulations in reproducing observations. Our study shows that progress in modeling how Greenland melt affects the nearby ocean is best achieved by improving model resolution so that small-scale processes can be well represented.

1. Introduction

The Greenland Ice sheet has been losing mass over the last two decades, as detected with gravimetric satellite missions (Gravity Recovery and Climate Experiment, GRACE, and its successor GRACE-FO), and other observations. For example, Bamber et al. (2018a) derived information on the components of Greenland freshwater flux (solid ice discharge, runoff, snowmelt) from satellite-based observations and regional atmospheric climate models. Between 2010 and 2018, the reconstructed ice mass loss of the Greenland ice sheet is 286 ± 20 Gt/year (Mouginot et al., 2019), and a rapid mass loss event followed in 2019 (Sasgen et al., 2020). This accelerated melt places the Greenland ice sheet as one of the main contributors to global sea level rise during the last two and a half decades and has caused a cumulative global mean sea level rise of 10.8 ± 0.9 mm since the 1990s (The IMBIE Team et al., 2020). Future projections indicate that the Greenland ice sheet contribution to global mean sea level rise could reach 13 cm (on average, relative to the baseline of 1995–2014) by the end of the 21st century

when looking at the fossil-fueled development (SSP5-8.5) Intergovernmental Panel on Climate Change (IPCC) scenario and 8 cm for the intermediate greenhouse gas emissions scenario (SSP2-4.5) (Fox-Kemper et al., 2021).

Regional sea level changes could be determined by tide gauge records; however, this is problematic since tide gauges see both trends from Glacial Isostatic Adjustment (GIA) and auxiliary local vertical land motion, along with local ocean effects (Brunnabend et al., 2015). In addition, they are sparsely distributed, particularly in the region around Greenland, and are often not located in the regions where the largest signal is expected. Radar altimetry (e.g., gridded products from Archiving, Validation and Interpretation of Satellite Oceanographic data, known as AVISO) provides absolute sea level heights but is hampered by sea ice and cannot distinguish between mass addition and steric changes (i.e., changes due to volume expansion caused by temperature and/or salinity variations). Lastly, there are inverse approaches seeking to combine GRACE and altimetry data to estimate mass and steric sea level components (Rietbroek et al., 2016; Uebbing et al., 2019). Traditionally, observed ocean mass changes from GRACE and geometric sea level change from altimetry are processed independently and only combined in a second step in order to construct sea level budgets. In contrast, an inverse approach (Rietbroek et al., 2016; Uebbing et al., 2019) combines both data sets in a joint estimation step allowing to consider available error information of the individual input data sets when deriving the sea level budget. The inversion uses mass and steric "fingerprint" patterns derived by employing the sea level equation, which allows to related variations in (ice) mass loading to corresponding changes in sea level (Farrell & Clark, 1976) and steric patterns from a principal component analysis of steric reanalysis data. In the inversion, these mass and steric patterns are then adjusting to fit GRACE and altimetry observations in a way that is consistent with self-attraction and loading (SAL) theory (Farrell et al., 1973; Kuhlmann et al., 2011).

Signatures of glacial melt can also be simulated in numerical ocean models. One way to study the effects of the Greenland melt on the ocean is to perform so-called water hosing experiments, that is, model experiments where Greenland freshwater flux is artificially added to the ocean (Gerdes et al., 2006; Kleinen et al., 2009). Studies performing hosing experiments and looking at increased melting of the Greenland and Antarctic ice sheets show that flows directed into the North Atlantic have greater impacts on various ocean basins than those directed into the Southern Ocean (Stammer, 2008). Brunnabend et al. (2015) included a constant Greenland mass loss rate of 200 Gt/year (6.3 mSv, for reference 1 mSv is equal to 31.6 Gt/year) in the Finite Element Sea Ice-Ocean Model (FESOM). After a 50-year simulation, the Northeast American coast experienced a sea level rise of 6–8 cm due to ocean mass redistribution, which is connected to a simulated decrease of the Atlantic Meridional Overturning Circulation (AMOC). Many Greenland freshwater studies have been carried out within the framework of the Forum for Arctic Modeling and Observational Synthesis (FAMOS, e.g., Dukhovskoy et al., 2019; Proshutinsky et al., 2016). From meltwater tracing experiments and further Greenland meltwater impact studies, it has been demonstrated that meltwater originating from the Southwest and West Greenland Shelf is moving into the interior of the Labrador Sea (Böning et al., 2016; Dukhovskoy et al., 2016; Gillard et al., 2016). Devilliers et al. (2021) have studied the effects of realistic melting rates in a coupled climate model and found freshening and cooling effects around Greenland. To realistically simulate the effects of Greenland freshwater, the ocean model needs an adequate horizontal eddy-resolving/eddy-permitting resolution especially in the coastal zones (Gillard et al., 2016; Wekerle, Wang, Danilov, et al., 2017). For the region around Greenland, this eddy-permitting resolution is around 5–10 km.

In terms of surface restoring, hosing experiments with a prescribed atmosphere may provide a less complete picture of freshwater distribution, temperature and salinity perturbation and, eventually, changes in sea level as compared to coupled ocean-atmosphere simulations (Swingedouw et al., 2013). The main weakness of ocean-only simulations for the performance of hosing experiments is the salinity restoring at the surface, which limits the direct signal of the hosing, and the sea surface temperature restoring, which limits the potential feedbacks and adjustments of temperature and circulation. However, the advantage of ocean-only simulations is that they are less noisy as there is no coupling with other model components, for example, the atmosphere. Ocean-only simulations can therefore be performed at higher resolution and more easily compared with observations. Since our focus here is on comparing simulations to a few decades of ocean data (only), we chose to impose atmospheric forcing from a reanalysis. Here, we only consider surface salinity restoring, which implies that no heat is added or removed in the meltwater entrance zones.

To make sure ocean models are responding to melt properly, simulated ocean fields such as temperature and salinity are compared with in situ observations and reanalysis. Argo floats, ship CTD profiles and other hydrographic

survey measurements are the only direct observations at depths. Ocean reanalyses provide a synthesis of many different observations and the essential model physics by incorporating numerical models; they provide variables on grids, but the reanalysis must be a compromise and will never reproduce a single observed field particularly well (Hoteit et al., 2018; Stammer et al., 2016).

Several studies have focused on transports such as the AMOC, for example, Kienert and Rahmstorf (2012), X. Wang et al. (2012), Ackermann et al. (2020), and Sidorenko et al. (2020). Our focus here, however, is whether Greenland freshwater flux is already visible in regional sea level observations (although we do not provide a formal detection-attribution study here). In this paper, we apply ocean modeling including and excluding Greenland freshwater on two meshes with different horizontal resolution. We focus on assessing the realism of the simulations by comparing output with observational data sets at the surface, such as altimetry and GRACE products, and at deeper layers, such as information from Argo floats and reanalysis data. We concentrate on three-dimensional temperature and salinity fields, steric heights and sea level anomalies. The central hypothesis of this study is that the Greenland freshwater signature is responsible for reducing the differences between model output and observations/reanalysis in the upper ocean. The scientific question we address here is: How important is (a) Greenland discharge and (b) model resolution to representing the ocean state and variability in FESOM compared to observations and reanalyses?

Section 2 describes the FESOM model with accompanying experiments, the freshwater data set and data sets used for comparison with the model output. In Section 3, we compare the model results for salinity, temperature, steric heights and sea level anomalies with different observational data products. Section 4 discusses the results with respect to the visibility of Greenland melting signatures in the North Atlantic as well as the mesh resolution.

2. Methods and Data

To assess whether melting signatures are visible in observations, we look at the surrounding ocean of the Greenland coast and define six regions - whose boundaries roughly follow the isobaths (lines of equal depth) - covering the Greenland Sea in the East, Denmark Strait and parts of the subpolar North Atlantic in the South and Southeast, parts of the Labrador Sea in the Southwest, Davis Strait, and Baffin Bay in the West (see Figure 1). Additionally, we look at three coastal regions in the East, South, and West.

2.1. Model Setup

For this study, the global multi-resolution sea ice-ocean model FESOM (Finite Element Sea Ice-Ocean Model, version 1.4, Q. Wang et al., 2014) is used. In the horizontal direction, FESOM uses an unstructured triangular surface mesh. In 3D, prisms are formed from the 2D surface nodes, which are cut into tetrahedral elements. The model configuration is based on z-level grids with 47 vertical layers of varying thickness (the upper 100 m depth range has a vertical resolution of 10 m). The ocean model is coupled to a dynamic-thermodynamic sea ice model (Danilov et al., 2015; Timmermann et al., 2009). The thermodynamic part is based on the formulation of Parkinson and Washington (1979), and includes a prognostic snow layer accounting for the effect of snow-ice conversion due to flooding (Owens & Lemke, 1990). It assumes a linear temperature profile in the ice and the snow, and is thus a 0-layer model. The dynamic part of the sea ice model uses the elastic-viscous-plastic (EVP; Hunke & Dukowicz, 1997) rheology. Prognostic variables are ice and snow thickness, ice concentration and ice drift velocity. The sea ice model is discretized on the same surface mesh as the ocean model.

FESOM is initialized by using temperature and salinity climatologies provided by the Polar Science Center (PHC 3.0; http://psc.apl.washington.edu/nonwp_projects/PHC/Climatology.html, last access: 21 September 2022); temporal coverage: 1900–2014; Steele et al. (2001) and it is forced with atmospheric variables, such as zonal and meridional wind at 10 m height, air temperature at 10 m height, specific humidity at 10 m height, precipitation and downward longwave and shortwave radiation taken from the JRA-55 reanalysis (Kobayashi et al., 2015). In addition, we specify monthly river runoff (also from JRA-55), which is uniformly distributed within a radius of 300 km from the river mouths.

FESOM is designed for unstructured multi-resolution meshes. One advantage of using this type of mesh is that areas of interest can be assigned a higher horizontal resolution than others. Global simulations with a regional focus can be carried out, which avoids the need to define boundary conditions and nesting as done in other
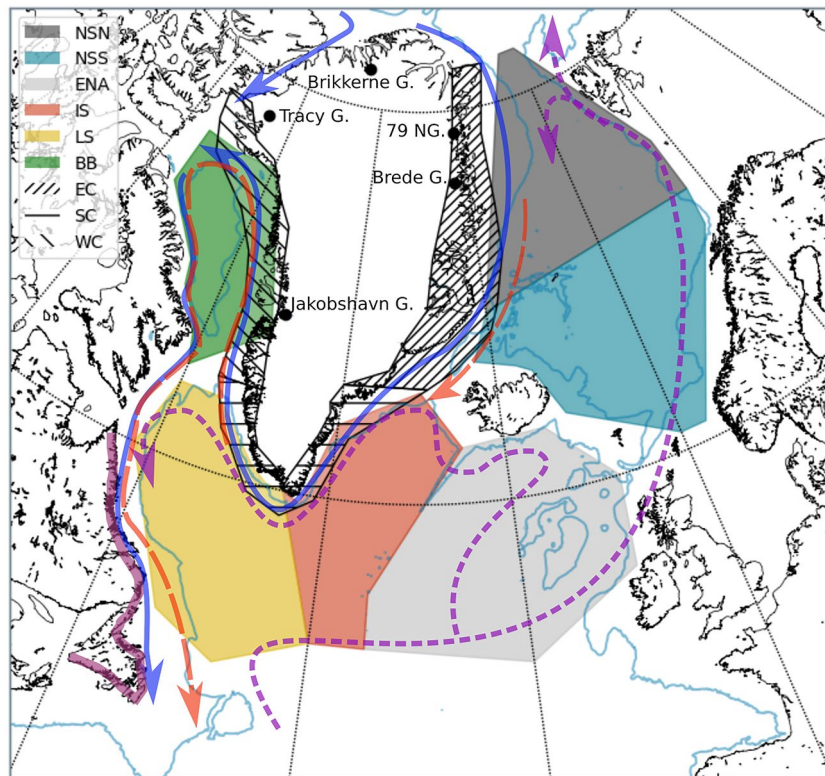
Figure 1. Selection of study regions in the North Atlantic based on the ocean bathymetry. The light blue line represents the depth level in 1,000 m (Schaffer et al., 2016); The six regions are the Nordic Seas North (NSN), Nordic Seas South (NSS), Eastern North Atlantic (ENA), Irminger Sea (IS), Labrador Sea (LS), and Baffin Bay (BB). We define three coastal areas: East coast (EC), South coast (SC) and West coast (WC). Additionally, some prominent glaciers are marked, such as Jakobshavn Glacier (JG), Tracy Glacier (TG), Brikkerne Glacier (BkG), 79°N Glacier (79°N) and Brede Glacier (BG). Major currents are represented including warm Atlantic waters (purple dashed lines), mixed Atlantic waters (orange dashed lines), and cool and fresh waters from the Arctic (blue lines). The coastal zone of Newfoundland and Labrador are shown in magenta (Southwest of Greenland).

models. In this study we performed simulations on two different meshes: (a) a low resolution mesh with 24 km resolution in the North Atlantic and Arctic Ocean (in the following we call it LOW) and (b) a high resolution mesh where resolution is equal to half of the local Rossby radius in the Atlantic and Arctic Oceans, capped at 6 km (in the following we call it HIGH) (see Figures 2a and 2b). The other ocean areas have a resolution of one degree. The spatial scales of baroclinic ocean mesoscale eddies can be broadly characterized by the first baroclinic deformation radius R. This radius can be approximated by $R = 1/(f\pi) \int_{-H}^{0} N(z)dz$, with $N(z) = \sqrt{-g/\rho \cdot d\rho/dz}$, where N is the buoyancy frequency to be integrated from seafloor ($-H$) to the surface, f is the Coriolis parameter, g is gravitational acceleration, and ρ is the sea water density (Chelton et al., 1998). According to Hallberg (2013), the ocean model resolution needs to be at least twice the Rossby radius to be able to resolve eddies. This is not the case in our HIGH configuration, which is only eddy-permitting in some regions of the northern North Atlantic like Baffin Bay, but not on the Greenland shelf regions due to a smaller Rossby radius (see Figures 2c and 2d). However, using a similar FESOM simulation (4.5 km instead of 6 km mesh resolution in the Nordic Seas), Wekerle, Wang, Danilov, et al. (2017) showed that the East Greenland Current, which transports freshwater from the Arctic, is well represented in the model regarding its core position when comparing to observations. The strategy of mesh design following the local Rossby radius applied for our high resolution mesh has been described by Sein et al. (2017). Note that the higher horizontal resolution in HIGH is mostly able to resolve the geometry within the fjords of the Greenland coast (Figure 2).

We apply a surface salinity restoring to the monthly PHC climatology in our simulations (according to the formula for the surface restoring freshwater flux $F_{rest} = V_{piston} \cdot (SSS_{model} - SSS_{clim})/SSS_{model}$, where SSS is the sea surface salinity, and V_{piston} the piston velocity, see Equation 1 in Behrens et al. [2013]). The restoring helps to avoid local
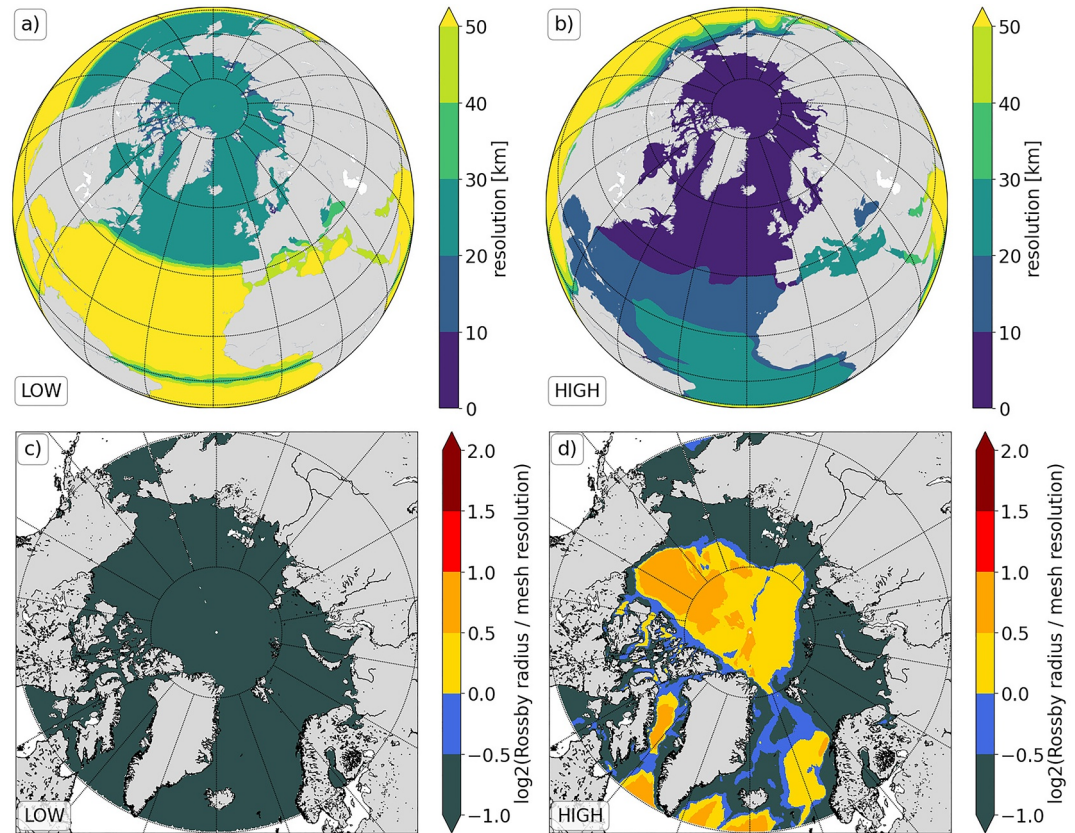
Figure 2. Global mesh resolution (in km) for (a) LOW and (b) HIGH; The relation of first Rossby radius from the Arctic Regional Climatology north of 60°N (Seidov et al., 2015) to the corresponding mesh resolution in log 2 is shown for LOW (c) and HIGH (d). This representation allows to interpret the colorbar as follows: if the model configuration is eddy-resolving (the value is above 1), eddy-permitting (between 0 and 1), or does not resolve eddies (below 0) as in Wekerle, Wang, Danilov, et al. (2017).

salinity trends that can occur in response to inaccuracies in, for example, precipitation (Q. Wang et al., 2018). However, we use a very small piston velocity of 7.9274e−08 m/s, which defines the strength of surface salinity restoring (Q. Wang et al., 2018), to retain the freshwater flux from the Greenland ice sheet. This piston velocity value is smaller than values commonly used in ocean models (Danabasoglu et al., 2014). In addition to this, precipitation is reduced by 10% in the North Atlantic to keep the AMOC in a realistic range according to the method by Behrens et al. (2013). The damping due to restoring is large, but less than the freshwater flux supplied (see Figures S1 and S2 in Supporting Information S1, and Section 4).

FESOM (version 1.4) has been extensively used and validated with focus on heat/volume transports (Q. Wang et al., 2020; Wekerle, Wang, Danilov, et al., 2017), mesoscale circulation in the upper ocean (Wekerle, Wang, Danilov, et al., 2017), East Greenland current circulation (Richter et al., 2018; Wekerle, Wang, Danilov, et al., 2017), vertical temperature/salinity distribution at Fram Strait or along a section in Labrador Sea (Scholz et al., 2014; Wekerle, Wang, von Appen, et al., 2017).

2.1.1. Greenland Freshwater Model Experiments

We perform two different model experiments: (a) the "realistic" run including Greenland freshwater (in the following we call it GF) and (b) the reference run excluding Greenland freshwater (in the following we call it NGF). The freshwater flux is distributed horizontally from the Greenland coast with a distribution radius of 60 km (see Figure S3 in Supporting Information S1) and is introduced in the ocean surface layer (top model layer).

The Greenland meltwater input data set is obtained from Bamber et al. (2018b). We use the total Greenland fresh-water flux, not just its surplus. The solid ice discharge is treated the same way as the liquid components (runoff of

tundra and runoff of Greenland ice sheet) and a slower melting of the solid ice component is not (yet) considered. Thus, the transport of icebergs is neglected as well as the direct thermodynamic impact of their melting through latent heat fluxes (Marson et al., 2021).

When including the Greenland freshwater data set in the model, we modify the salinity distribution but not the temperature distribution. Temperature variations arise due to the dynamic response of the freshwater input. Note that we use a salinity restoring as described in the section before, which slightly modifies the applied Greenland runoff. Figure S2 in Supporting Information S1 show maps of both fluxes, Greenland freshwater flux and salinity restoring, and their ratio.

2.2. Observations and Other Products

2.2.1. Argo Floats

We compare simulated temperature (T) and salinity (S) with data from Argo floats for the time period between 2005 and 2016 (https://www.ncei.noaa.gov/access/metadata/landing-page/bin/iso?id=gov.noaa.nodc:Argo-Monthly, last access: 23 June 2019) (Argo, 2020). We select five study regions around Greenland for the comparison with Argo floats occurring within each polygon. Baffin Bay is not selected for the Argo comparison as very few floats are available there. The shape of the regions roughly follows the bathymetry from Schaffer et al. (2016), and aims to cover regions which have sufficient float coverage, and where we expect a coherent ocean response. The comparison of the model output with the Argo floats is done in two steps: (a) Interpolating FESOM model output to each Argo position; (b) Aggregating the (modeled and observed) profiles within each polygon and given depth level (0–50, 50–100, 100–250, 250–500, 500–750, 750–1,000, 1,250–1,500, 1,500–1,750, 1,750–2,000 m).

2.2.2. GRACE and Altimetry

There are several methods to use gravimetric data together with altimetry in order to estimate Greenland ice mass balances. We follow the fingerprint inversion method by Rietbroek et al. (2016) since this enables us to separate steric expansion from mass variations in a more consistent way than just differentiating altimetric and ocean mass maps. Combining GRACE gravimetric data and sea surface heights from altimetric data in a joint inversion analysis allows us to study the Greenland mass balance and sea level budgets of the North Atlantic (Rietbroek et al., 2016; Uebbing et al., 2019). The inversion method fits spatial modes of steric and mass sea level change to altimetric data and GRACE by estimating the temporal variations (one for each mode). With this technique, steric and mass-driven sea level contributions are estimated simultaneously and are thus consistent in terms of ocean bottom pressure, sea surface height and solid earth response. We use GRACE data from 2002 to 2016. The altimetric part is based on Envisat (2002–2012), SARAL/AltiKa (2013–2016), Jason1 (2001–2012), and Jason2 (2008–2016) (Scharro et al., 2013). We follow the inversion method and update the settings by Uebbing et al. (2019): for GRACE data we use ITSG2018 (Kvas et al., 2019; Mayer-Gürr et al., 2018) instead of GFZ RL05a (Dahle et al., 2013); for altimetry we add Envisat and SARAL/AltiKa data to the Jason missions; for estimating the steric sea level fingerprints, we use the Ocean Reanalysis System 5 (ORAS5, Zuo et al. (2019), see Section 2.2.3) instead of the Ocean Reanalysis Pilot 5 (ORAP5, Zuo et al., 2017). Envisat and SARAL/AltiKA are advantageous here as these missions cover high latitude regions and, thus, our study area. From the inversion output, we extract steric height changes.

For evaluating simulated sea level anomalies, we use the gridded AVISO data set. The Ssalto/Duacs altimeter products are produced and distributed by the Copernicus Marine and Environment Monitoring Service (CMEMS) (https://marine.copernicus.eu, last access: 9 March 2021).

2.2.3. Ocean Reanalysis

We use three-dimensional fields of temperature and salinity of ORAS5 provided by the European Centre for Medium-Range Weather Forecasts (ECMWF) (https://www.cen.uni-hamburg.de/icdc/data/ocean/easy-init-ocean/ecmwf-oras5.html, last access: 15 April 2021). Furthermore, we derive steric height changes following the Thermodynamic Equation of Sea Water 2010 (TEOS-10) via the Gibbs SeaWater (GSW) Oceanography Toolbox (McDougall & Barker, 2011). Steric heights, relative to a reference water column, are defined as

$$sh(S, T, P) = \int_{-H}^{0} \frac{\rho(S, T, P(z)) - \rho(S_0, T_0, P(z))}{\rho(S_0, T_0, P(z))} dz, \tag{1}$$

where ρ is the ocean density, $S_0 = 35$ psu is reference salinity and $T_0 = 0°C$ is reference temperature. Steric height anomalies are referenced to the multi-year mean of 2005–2012. No further distinction between thermosteric and halosteric contributions is made here.

ORAS5 uses the Nucleus for European Modeling of the Ocean (NEMO) ocean model in a global setup (0.25° horizontal resolution on 75 vertical levels). Observations that are used in the ORAS5 system are sea surface temperatures, sea level anomalies (AVISO) and in situ data such as Argo and XBT measurements. As ORAS5 additionally includes sea ice observations and has a relatively high horizontal resolution in the Arctic of up to 9 km, it seems suitable for high latitude studies (Carton et al., 2019; Zuo et al., 2019). In the tropics, the horizontal resolution is about 25 km. ORAS5 consists of five ensemble members, which differ in the perturbation of initialization and the forcing data.

In this study, ORAS5 is used in two ways: (a) in the inversion approach, steric spatial modes from ORAS5 (ensemble mean) are used to fit GRACE and altimetry data; (b) for comparison with model output, ORAS5 (ensemble mean and variance) serves as observational basis.

2.2.4. Gridded In Situ Ocean Observations

In addition to the ORAS5 reanalysis, and for comparison with the performed model experiments, we use the salinity and temperature fields provided by the Coriolis Ocean Data set for Reanalysis (CORA, version 5.2, https://resources.marine.copernicus.eu/product-detail/INSITU_GLO_TS_REP_OBSERVATIONS_013_001_b, last access: 31 October 2022) (Cabanes et al., 2013; Szekely et al., 2019). This CORA product is disseminated within the framework of CMEMS. CORA includes a variety of different observation platforms, such as Argo floats, moorings, drifters, and CTDs. Here, we use the gridded CORA version. There is a considerable overlap between the data assimilated in ORAS5 and the CORA data set, so the differences between the two primarily reflect methodological, modeling, and gridding errors.

2.3. Fitness Metrics

We use the root mean square error (RMSE) and the Pearson correlation coefficient for evaluating the model simulations. To quantify the mean square error (MSE) between a model simulation and an ensemble of observations as in ORAS5 (and not only the ensemble mean), we follow the derivation by Stolzenberger et al. (2015), which has been originally introduced for validating a model ensemble. Changing this model-observation perspective for evaluating a simulation with an ensemble of observations, the MSE leads to

$$MSE(M, t_i) = \left(m(t_i) - \overline{o(t_i)} \right)^2 + \sigma^2(t_i),$$ (2)

where m is the model value at time t_i, and $\bar{o}$ and σ represent the mean and standard deviation of the observational ensemble at t_i. For better comparability, we use $RMSE* = \sqrt{\sum_{i=1}^{N} MSE(M, t_i)}$, where N is the number of time steps. The relative improvement (regarding the $RMSE*$ and the $RMSE$) of one model simulation (M_1) compared to another reference simulation (M_0) is defined as $RMSS(*) = 1 - \frac{RMSE_{M_1}(*)}{RMSE_{M_0}(*)}$.

Furthermore, we determine the added value ρ^+ that describes the increase in total correlation due to model experiment A (and a corresponding observation) given model experiment B (Glowienka-Hense et al., 2020). The added value of the GF-experiment given the NGF-experiment is defined as

$$\rho^+ = \frac{(\rho_{12} - \rho_{13}\rho_{23})^2}{1 - \rho_{23}^2},$$ (3)

where the index 1 denotes the Argo float observation, 2 the GF-experiment and 3 the NGF-experiment. If ρ^+ is zero, there is no added value to the GF-experiment.
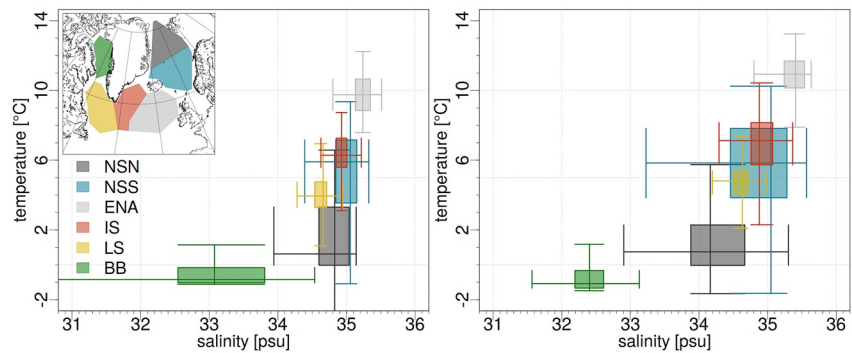
Figure 3. Salinity and temperature distribution for each polygon (see Figure 1 for region names) based on the ORAS5 ensemble mean (left) and HIGH (right) for 1993 to 2016. In these two-dimensional Box-Whisker plots, single information about salinity and temperature variability (averaged over the upper 100 m) are summarized. The box edges represent the lower and upper quartiles and the vertical and horizontal lines show the whiskers with 1.5 times the interquartile range. Possible outliers are not displayed. Highest temperature and salinity values are found in the ENA region (see Figure 1), lowest are found in BB (on average).

3. Results

3.1. Salinity and Temperature

The salinity and temperature distribution in the top 100 m for each region based on ORAS5 and model HIGH is shown in Figure 3. In region ENA, we can expect the highest values for temperature (median ca. 9.8°C for ORAS5/11°C for HIGH) and salinity (median ca. 35.2 psu for ORAS5/35.4 psu for HIGH). One reason for this is the incoming warm Atlantic waters passing ENA, and further, IS and LS. While the temperature distribution for BB is rather tight (minimum-maximum range is 2°C for ORAS5), the interquartile range of salinity is larger than 1.5 psu. In ORAS5, the salinity range is even wider for BB.

Although the Greenland freshwater is injected only at the ocean surface in our experiments, effects can be seen in deeper ocean layers (average of upper 100 m depth in Figure 4 and single levels in Figure S5 of Supporting Information S1). Including GF makes the surrounding of Greenland and especially Baffin Bay less salty. Not only does the West coast show differences of 0.5 psu and more, but also the Northern areas including, for example, Brikkerne Glacier, and the East including, for example, Brede Glacier (see Figure 1 for locations). The effects of GF are also visible at the Northern coast of Newfoundland and Labrador. The effects on salinity of GF in LOW and HIGH models have a similar structure. For temperature, the inclusion of GF has a warming effect along the western coastline of Greenland, from Jakobshavn Glacier up to the Northwest including Tracy Glacier. For LOW, this signal at the West coast is more pronounced with values up to 1°C compared to HIGH. This warming effect causes the temperature to rise above freezing earlier in the year by about 1.1 months (on average) for LOW, and by 1.6 months for HIGH. There are even winter seasons, for example, between 2003 and 2004, where the temperatures in the GF-experiment stay above 0°C at the Western coastal zone. Castro de la Guardia et al. (2015) explain this warming effect in Baffin Bay with rising sea surface heights (SSH) due to the increased runoff along the West Greenland coast. The SSH gradient steepens between the West Greenland coast and Baffin Bay center, which (positively) enhances the northward freshwater transport via the West Greenland current from Irminger Sea. This results in lower salinity in Baffin Bay and may lead to further sea surface elevations and thus stronger Baffin Bay gyre circulation, and further ocean warming (Castro de la Guardia et al., 2015). As described in Section 2.1.1, we do not modify temperature when introducing Greenland freshwater. The warming effect we see here is due to dynamic reasons. At the south and southwest of Greenland, we find an opposite pattern in both LOW and HIGH, that is, the upper ocean gets cooler when including GF. For HIGH, this signal is also visible in the Southeast, in the LS and further south. While the cooling effects of 0.2°C in LOW directly start at the coastal zone, there is distance of ca. 60–100 km when this pattern occur in HIGH. The positive pattern in LOW south of 60°N and between 20 and 40°W does not appear in HIGH. This could be related to the eddy dynamics which are resolved in HIGH (see Section 4). The salinity differences in Baffin Bay, around the Greenland coast are significant as well as the temperature changes at the west and partly at the south of Greenland.
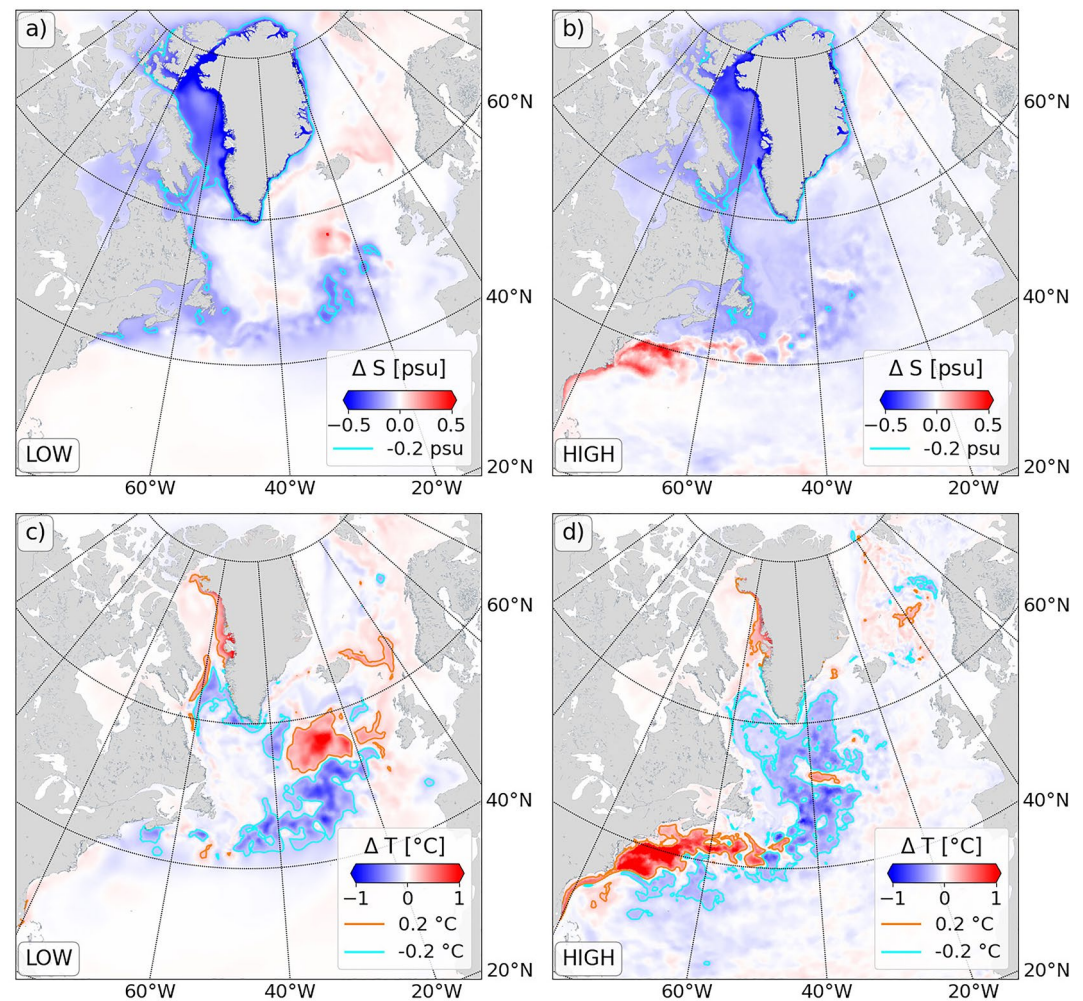
Figure 4. Differences between GF simulation and reference simulations for LOW (a, c) and HIGH (b, d) averaged over the upper 100 m for the time period 1993–2016. The differences are shown for salinity (top) and temperature (bottom). Blue shadings represent cooling and freshening effects due to GF. Differences in selected depth layers are displayed in Figure S5 of Supporting Information S1. Differences for each year between 1993 and 2016 (averaged over the top 100 m) are shown in Movie S1.

The ORAS5 and CORA variability for salinity in the Nordic Seas is small compared to the variability of the model simulations (Figure 5), for example, the ratio of the standard deviations of CORA to the standard deviation of LOW GF is 0.27 in NSN. In the Labrador Sea, the trend of simulations and ORAS5 is of opposite sign until 2001 and after that shows a bias of up to 0.2 psu (for HIGH). LOW shows too high salinity compared to ORAS5 at the south coast of Greenland (SC) and changes to underestimate it in mid 2004, whereas HIGH is in line with ORAS5 in the 1990s. The freshening signal since 2009 at ENA and the negative anomalies until 2016 are consistent with, for example, the studies by Holliday et al. (2020) and Tesdal et al. (2018).

For temperature in the Nordic Seas, we observe a positive trend in both ORAS5 and the model simulations in the upper 100 m (Figure 6). This is visible in the GF- and NGF-experiments. For areas in the South (ENA, IS, LS, SC), we see a temperature increase in the 1990s and a decrease since 2013 (u-shaped evolution). In the Nordic Seas, FESOM overestimates the ORAS5 time series until 2001/2002 and slightly underestimates it since then, at least in NSS. Here, HIGH is closer to CORA compared to LOW (by 24%). For EC, the positive temperature trend is captured by the model simulations (RMSE is 0.245°C for LOW), but the ORAS5 plateau between 2001 and 2006 cannot be reached by either LOW or HIGH.

The influence of Greenland meltwater on the surrounding ocean is small in most of the considered regions (Figures 5 and 6). However, there are time intervals and areas where the Greenland freshwater plays a more
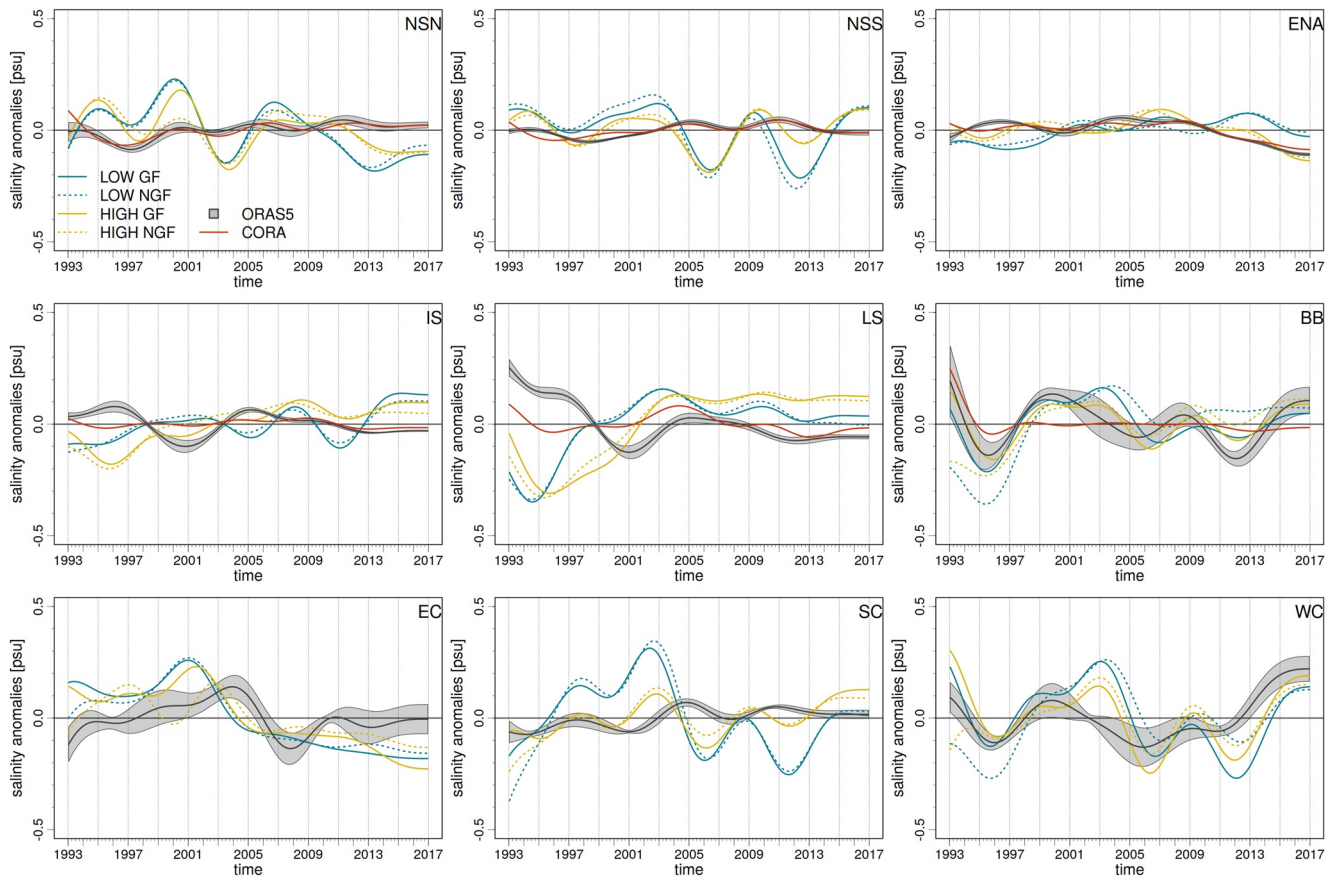
Figure 5. Interannual signal (5 years filter) of salinity anomalies for all considered regions according to Figure 1 averaged over the upper 100 m. The gray shading is based on the ORAS5 ensemble uncertainty, the thick gray line represents the ensemble mean. The reference time period for determining the anomalies is from 1993 to 2016.

important role. The largest differences between the GF and the NGF experiments can be seen at the East and West coast, and Baffin Bay. For the latter, we find for salinity an improvement of the GF-experiment (in contrast to NGF-experiment) of 34.1%, when comparing with ORAS5, and up to 40%, when comparing with CORA. For temperature, the effects are also visible, but for BB, NGF fits slightly better to ORAS5. Freshwater effects for salinity at the eastern coast can be identified, especially at the beginning and end of the time series. For EC, the negative salinity trend between 2003 and 2008 can be detected in all products (Figure 5). This decrease is also visible in the simulated salinity values in SC and WC with slight temporal shifts. For WC, the GF- and NGF-experiment differ from each other, which can be connected with the freshwater increase used as input data (Bamber et al., 2018a). In the Southeast (IS), HIGH GF fits well to CORA and ORAS5 temperatures (RMSE of HIGH vs. CORA is ca. 0.2°C), whereas for salinity, the Greenland freshwater effect is not visible.

We compare FESOM simulations with data collected by Argo floats by interpolating the model output to the Argo float positions. The depth layers are categorized into nine vertical bins: 0–50, 50–100, 100–250, 250–500, 500–750, 750–1,000, 1,250–1,500, 1,500–1,750, 1,750–2,000 m. As Argo floats are rarely present in region BB, we focus on the other five regions. The RMSE is mostly larger for LOW compared to HIGH (Figure 7), indicating that the HIGH configuration is more realistic compared to LOW. For temperature, this is visible in IS and LS with an RMSE up to 0.7°C in LOW. An opposite example, where HIGH performs less well than LOW in terms of GF inclusion, is found for temperatures in the northern Nordic Sea area, where the RMS improvement is −11% and the added value is 1.1% in the upper 100 m. For salinity, the RMSE is slightly higher in the upper 100 m with values higher than 0.3 psu in region NSN. For this region, including Greenland freshwater improves the RMSE by 11% (for HIGH). For the Irminger Sea, HIGH performs slightly better, based on RMSE, for temperature and salinity in the upper 100 m. We find high correlations for HIGH, especially in the Southeast regions (IS). Here, the effect of GF is visible in HIGH at the upper 250 m with an added value of about 10% (Figure 8).
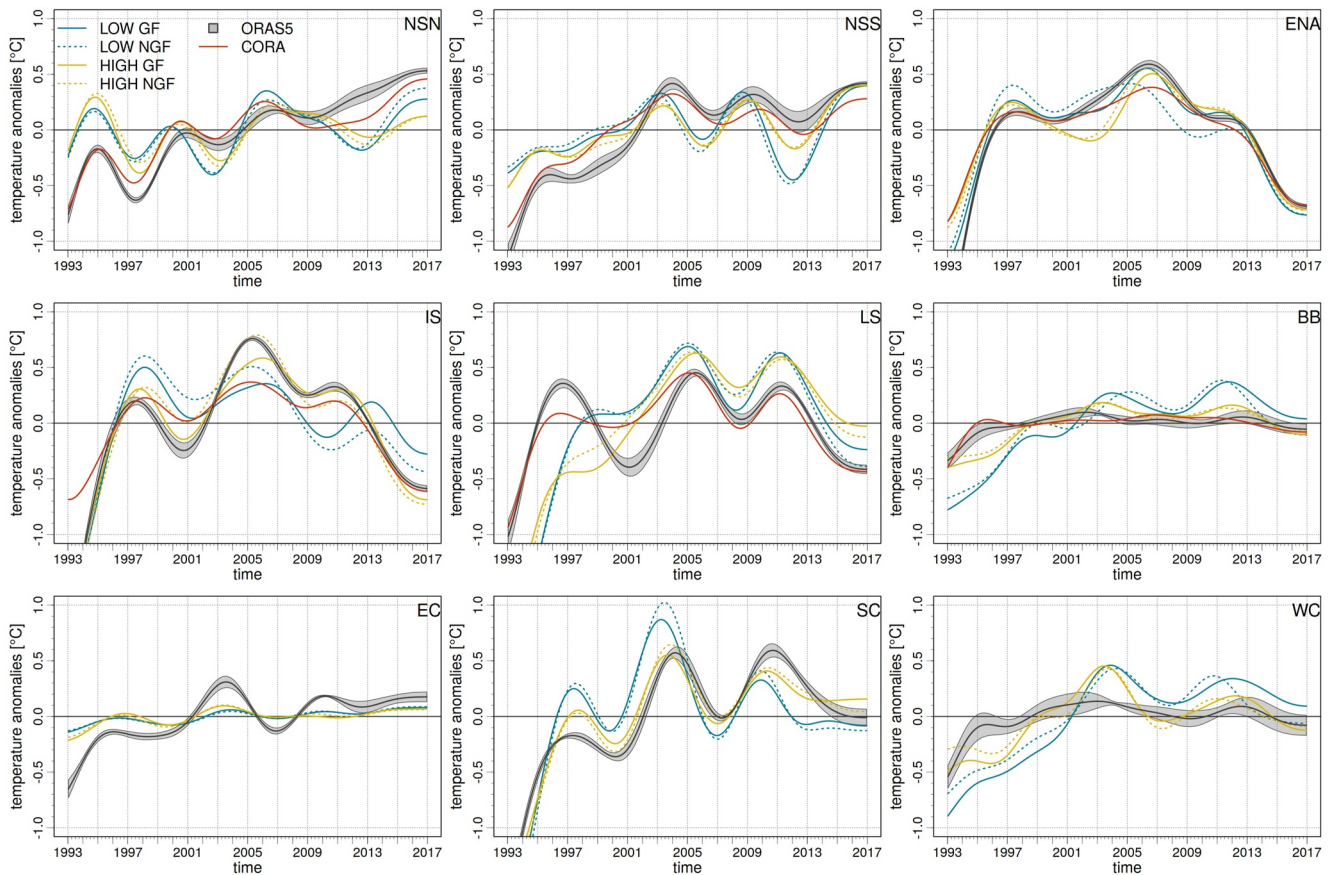
Figure 6. Same as in Figure 5 but for temperature.

Argo floats are sparsely represented in the first half of the time period. For example, in the NSN for 2005–2012 there are only 28 Argo floats per month compared with 62 per month between 2013 and 2016. To see how robust the coverage is in each region, we compare the last 5 years where more floats are deployed to the entire Argo period. To estimate an uncertainty, we bootstrap/resample ($n = 500$), over the number of Argo floats and calculate the RMSE, here for temperature in the upper 50 m. We find a systematic bias of ca. 0.4 °C between both time periods (see Table 1). The standard deviation is lower - by roughly $\sqrt{2}$ - for the longer time period. If there were 10 years more of Argo observations, this deviation would be reduced again by $\sqrt{2}$. For region LS, this reduction would be almost $\sqrt{5}$. When removing a 10% subset of the bootstrapping sample, this does not affect the median and the corresponding distribution. Vice versa, including an additional 10% of Argo floats in region A would also not affect the RMSE-distribution. We conclude that the systematic bias therefore does not result from the Argo float coverage within this polygon.

3.2. Steric Height Changes

Changes in steric heights reflect ocean volumetric expansion or contraction due to temperature or salinity changes. The calculation of steric heights is described in Section 2.2.3.

In the northeast of Greenland (NSN, Figure 9), we generally find a positive (significant) trend from around 2009 on, and further increasing around 2013. In contrast, for regions south of Greenland (ENA, IS, LS), we consistently observe a negative trend in steric height changes in recent years, which was preceded by an increase until the early 2000s. From 2013 onwards, cooling or saltiness or both dominate (the division into halo- and thermosteric changes are not shown here). In the west of Greenland, steric heights decrease until the end of the 1990s and
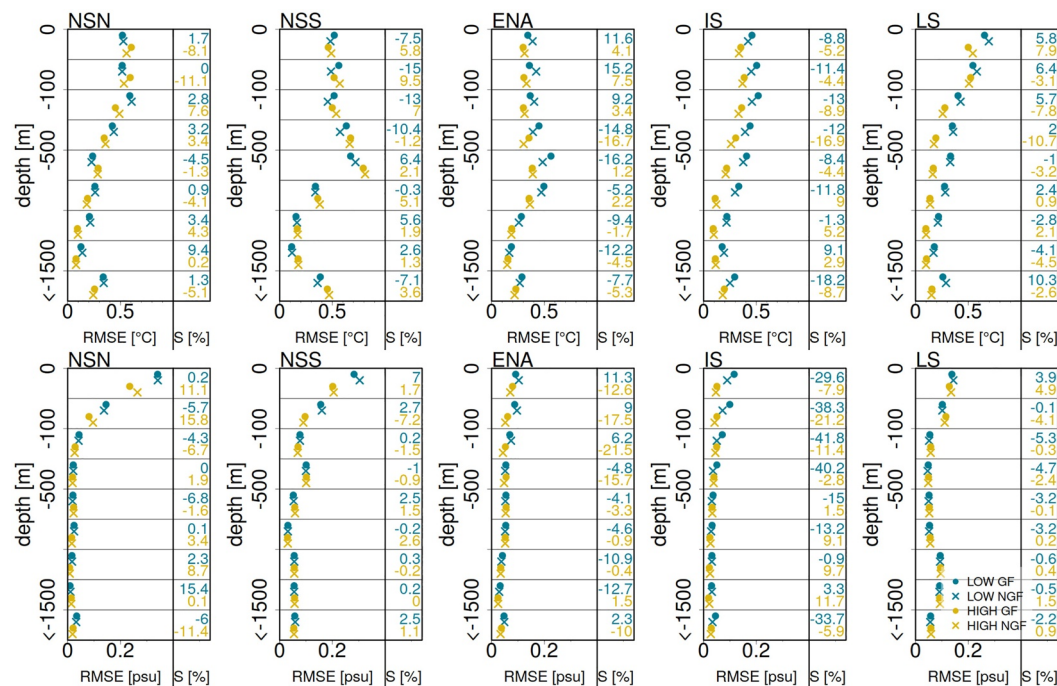
Figure 7. RMSE between each model experiment and the Argo float observations and relative improvement of the GF-experiment compared to NGF-experiment in percent (S, equal to RMSS) for temperature (top) and salinity (bottom). The overall RMSE (averaged overall depths and regions) for LOW/HIGH GF is 0.38°C ± 0.3°C/0.31°C ± 0.34°C for temperature and 0.07 ± 0.12 psu/0.06 ± 0.1 psu for salinity.
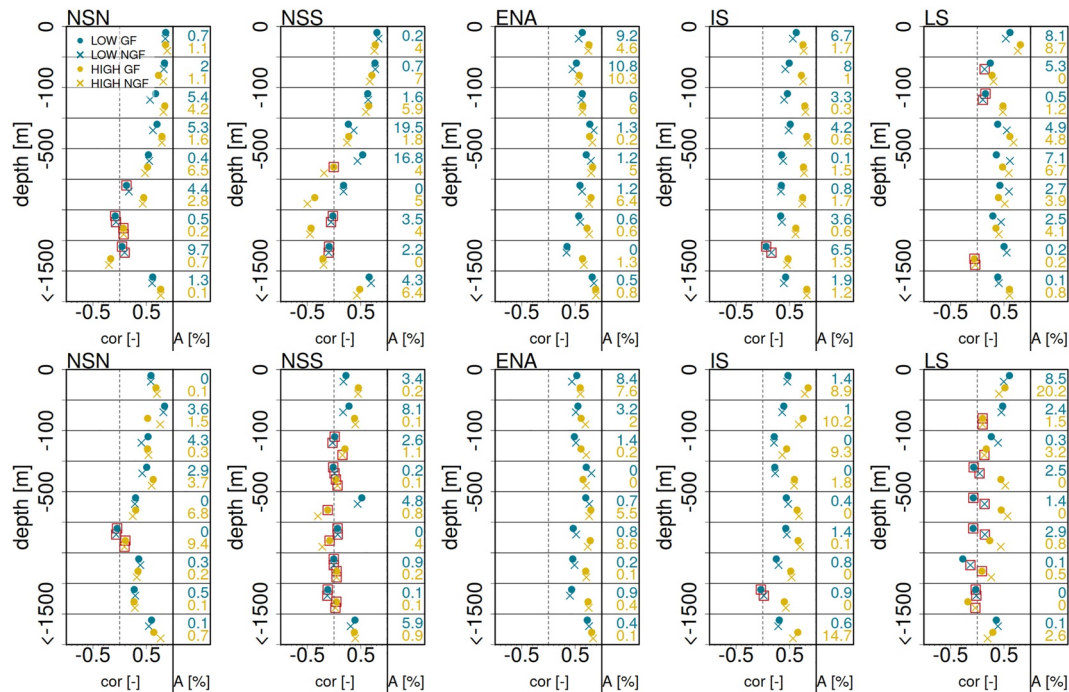

Figure 8. Correlations between each model experiment and the Argo float observations and added value of GF-experiment given NGF-experiment (A, equal to ρ^+, displayed as numbers in the right column) for temperature (top) and salinity (bottom). Red squares denote insignificant correlations based on the 5% significance level.

Table 1

Number of Argo Floats per Month (Average) for Each Region for the Argo Float Period (2005–2016)

	NSN	NSS	ENA	IS	LS
No. Argos per month	40	67	89	62	96
Bias (°C)	0.36	0.01	0.01	0.02	−0.02
σ-reduction (−)	1.40	2.05	2.14	1.41	2.17

Note. The systematic bias is based on the bootstrapping results when comparing the RMSE-median of the shorter time frame (2012–2016) with the entire Argo period for the upper 50 m. The σ-reduction represents the relative reduction of the standard deviation between both time periods. If there were 10 years more of Argo float observations, this deviation would be reduced again by $\sqrt{2}$ in the NSN region. The determination of these quantities is described in the text.

increase again until about 2011, at least as seen in the model simulation and in ORAS5.

As mentioned above, altimetry has been used in this study via an inversion process; we have fitted hundreds of leading modes of ORAS5 steric heights (fingerprints) to match altimetry corrected for GRACE. Steric height changes from the inversion thus often show a similar evolution as compared to the ORAS5 reanalysis, as both are constrained by altimetry, in particular at (sub-) seasonal scale but also for example, for the interannual signal in LS since 2011. For the inversion, high latitude regions are not covered by measurements for the whole time period due to sea ice. Thus, steric heights are not constrained well when there is only GRACE available. Based on sea ice concentration variability, we expect the best data coverage in the inversion for the regions NSS, ENA and IS. For most regions, comparing reanalysis and model simulations to altimetry reveals that spurious temperature or salinity biases create too strong SSH changes.

The month-to-month steric signal, which is defined as the difference between filtered and original data time series (see Figure 10), often lies within the uncertainty range of ORAS5. However, for some years for example, between 2010 and 2013 in region LS, we detect stronger month-to-month variability for ORAS5 compared to the inversion output. This region, together with region ENA and IS, are characterized by a stronger signal in contrast to the other areas, where maximum amplitude is up to twice as large as, for example, region BB. We find that the amplitude of the month-to-month signal of the inversion output is less pronounced compared to the ORAS5 ensemble mean.
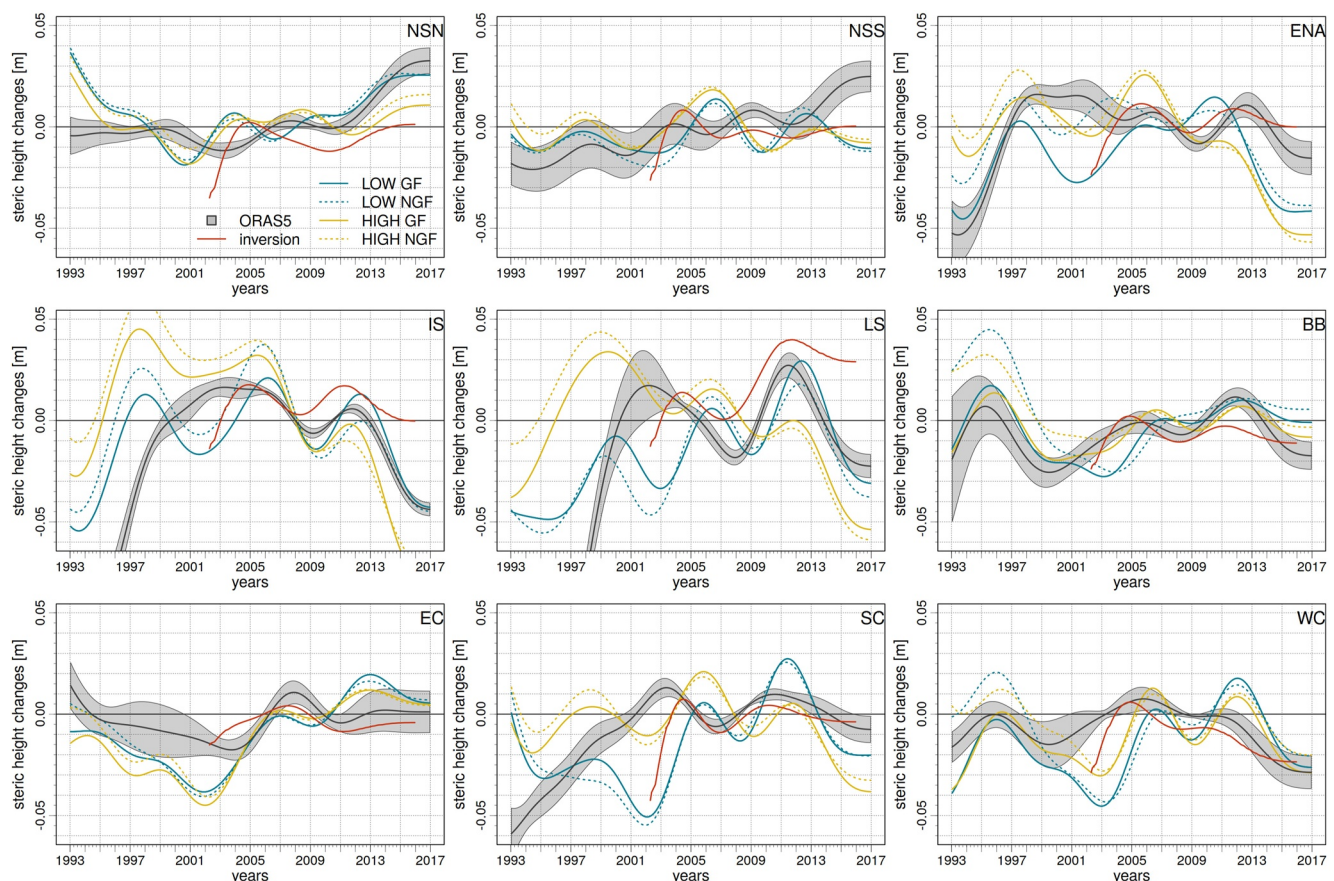

Figure 9. Interannual signal (5 years filter) of steric heights for all regions. The gray shading is based on the ORAS5 ensemble uncertainty, the thick gray line represents the ensemble mean. The inversion output is available since 2002 as it depends on the GRACE data.
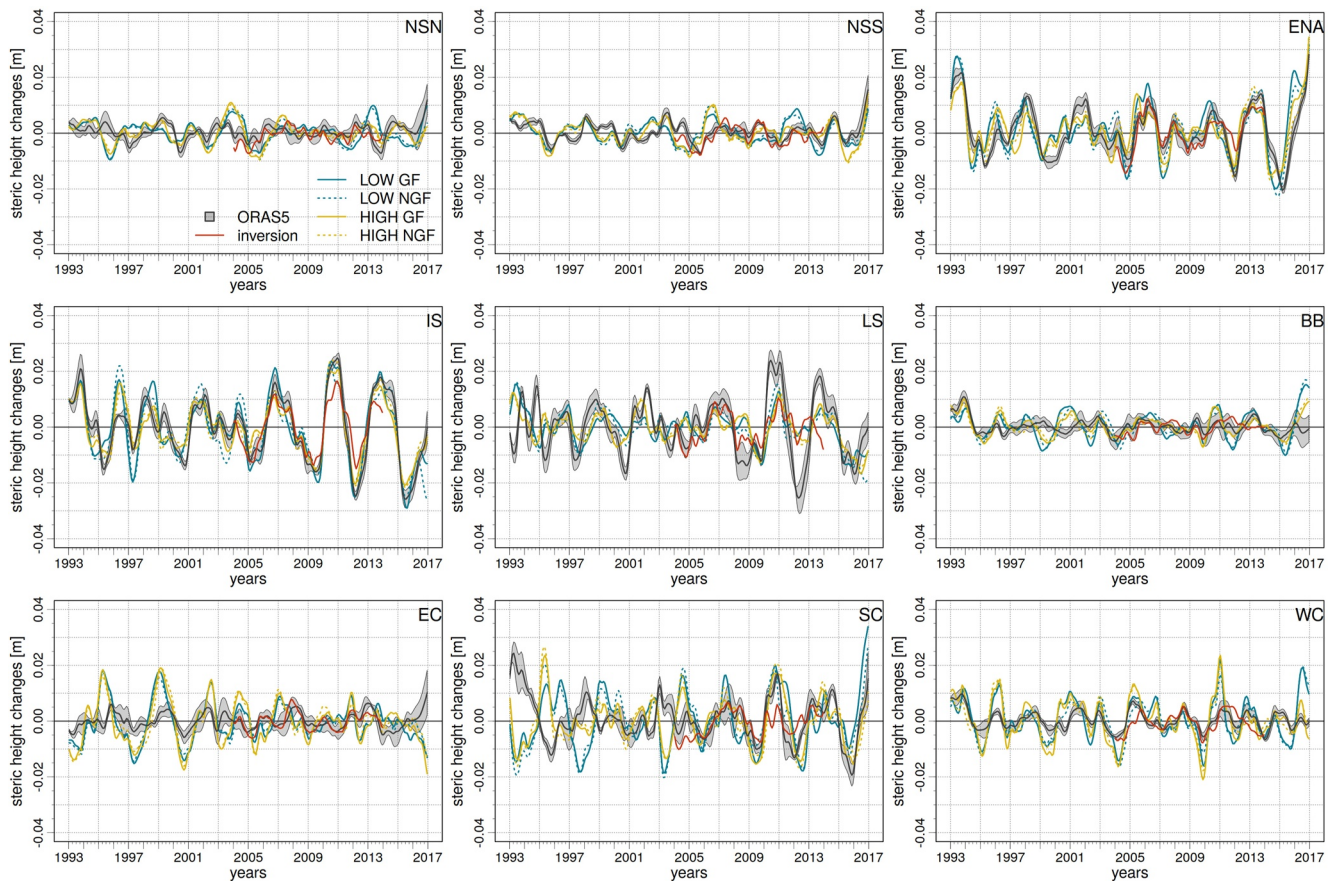
Figure 10. Month-to-month signal (excluding the seasonal cycle) of steric heights for all regions. Again, the gray area around ORAS5 is based on the ensemble uncertainty. Monthly variability is larger in the Southern areas than the Western and (North-) Eastern regions with phase and amplitude coinciding with each other. For the inversion output, the first and last 2 years of the time series are not displayed due to filtering effects.

Observations and simulations have a similar seasonal cycle for each region, which is mainly in phase (not shown here). The maximum amplitude in the model is about 2 cm for region NSN and BB. For NSN (BB), the modeled maximum amplitude is 0.8% (47%) larger than ORAS5 and 16% smaller (24% larger) than the inversion output. The more southern the region, the larger the amplitudes (up to 4 cm in region ENA and LS).

Comparing different model experiments, we find that there are areas where the model resolution seems to have a larger influence on steric sea level change than the Greenland meltwater influx, especially in more recent years (see Figure 9). In region ENA, since about 2008, experiments GF and NGF result in nearly identical variations for each LOW and HIGH run. In other words, Greenland freshwater seems to have negligible influence on steric heights in the considered regions. For earlier periods, however, the GF runs show smaller steric heights compared to NGF with a difference of ca. 2 cm. Another example is region NSN, where the LOW experiments are almost similar. To some extent, this is due to the choice of polygons for example, in the Nordic Seas, as GF is more concentrated along the east Greenland coast. The experiments in HIGH vary especially in the 1990s. The LOW steric heights are often within the ORAS5 ensemble spread, especially since 2012. For LOW, we find a correlation of 0.6 with the ORAS5 ensemble mean for the interannual evolution, whereas it is only 0.4 for HIGH. For the month-to-month signal in year 2003/2004, LOW and HIGH agree well with each other, but show higher values (up to 1 cm compared to the steric height observations).

There are, however, areas and time periods where adding Greenland meltwater has more pronounced effects on steric heights than from increasing model resolution. West of Greenland (BB) in the early 1990s, the LOW and HIGH GF experiments are closer to ORAS5 compared to the similarly proceeding reference runs. Including GF shows an improvement of the RMSE of about 37% for LOW and 32% for HIGH with respect to the ORAS5 ensemble spread. We find correlations of about 0.68 for LOW and 0.81 for HIGH compared to the ORAS5

ensemble mean and similar values when comparing to the inversion output. The impact of the freshwater is additionally evidenced by smaller RMSE values in LOW and HIGH. The freshwater behavior is not that clear in the month-to-month time series for these years, but all experiments are within the ORAS5 ensemble spread when looking at the years 2003–2006 and single years such as 2008. Another example for the freshwater effect is region IS, where the benefit from including GF is 28% (compared to the inversion output) for LOW and about 8% for HIGH (for ORAS5 and inversion).

3.3. Sea Level Anomalies

Greenland mass loss leads to regional sea level changes in the North Atlantic. Here, we compare sea level anomalies (SLA) from AVISO with the FESOM simulations. We apply a global mean correction for simulated sea surface heights in order to ensure the conservation of mass in the model (Böning et al., 2008; Greatbatch, 1994). We use Empirical Orthogonal Functions (EOFs) to describe the dominant modes of the observations and each model configuration. The local trend has been removed before computing the EOFs. The EOF analysis is based on the time period 1993–2016.

The first three EOFs explain respectively 20.1%, 11.9% and 4.0% of the total variance for AVISO, with similar values for the model simulations (Figure 11). EOF1 shows a low from Greenland Sea to Norwegian Sea and a high in the North Sea. EOF2 shows a high in the North Sea without visible areas of opposite sign. For EOF3, observations and simulations differ; however, all show a negative center along the western coast of Greenland and/or Baffin Bay. Negative patches in the subpolar gyre and the southwest of Greenland are not represented in LOW and turn positive in HIGH at some parts.

The EOF1 low in AVISO includes two patterns reflecting the bathymetry and, thus, the Nordic Seas. These patterns are less pronounced in the LOW simulations. Projecting the simulated data onto the AVISO basis vector, amplitude and evolution of the principal components (PCs) between simulations and observation fit mostly well together (Figure 12, and Figure S6 in Supporting Information S1 for different regions). For region NSN, we find correlations of about 0.81 for LOW versus AVISO and 0.9 for HIGH versus AVISO for PC1, also indicating that the HIGH version of the model fits altimetry better. The correlation values are even up to 0.07/0.02 (LOW/HIGH) higher for region NSS than for NSN. When reconstructing SLA based on the first three EOFs, the AVISO variability in regions ENA, IS and LS cannot be represented to the full extent by the LOW configurations with correlations (between AVISO and reconstructions) of less than 0.50 (Table S1 in Supporting Information S1).

From this EOF analysis, we cannot detect a uniform improvement in fit in the model compared with AVISO observations, when adding Greenland meltwater rates. As the sum of the first three EOFs explain 43.6% of the total variance (on average), potential energy in the remaining modes could be missed. We compare the model simulations with Aviso using the RMSE. In Baffin Bay and the Greenland Sea, RMSE values are below 5 cm for LOW and HIGH (Figure 13). In the South and southwest of Greenland, clusters with RMSE values of up to 10 cm are found in LOW, which are shifted further south in HIGH. Looking at the improvement of the RMSE when including GF shows generally similar structures in LOW and HIGH: the west, south and southwest of Greenland show a benefit of up to 20%. These areas are more contiguous in HIGH especially in the South and Southwest. Non-significant areas can be found north/northwest of Greenland and in the south of 50°N (40°E).

4. Discussion

One of the goals of this study was to find out how much of an impact the observed Greenland freshwater flow has on the surrounding ocean. Therefore, we included Greenland freshwater rates based on Bamber et al. (2018b) in the sea ice-ocean model FESOM. Our results suggest that including the Greenland melting rates lead to a warming and freshening effect in the upper 100 m along the western coast of Greenland. This comparison refers to the scenario where there is no Greenland melt at all. The analysis period is 24 years, from 1993 to 2016. Our results for the freshening effects in Baffin Bay and the Labrador Sea are consistent with the study by Dukhovskoy et al. (2016), Dukhovskoy et al. (2019), and Devilliers et al. (2021), who expect the largest differences in these regions.

Interestingly, the warming and freshening effects can be seen in the upper 100 m, although the Greenland freshwater flux is injected at the surface only. We hypothesize that a three-dimensional model of GF intrusion into
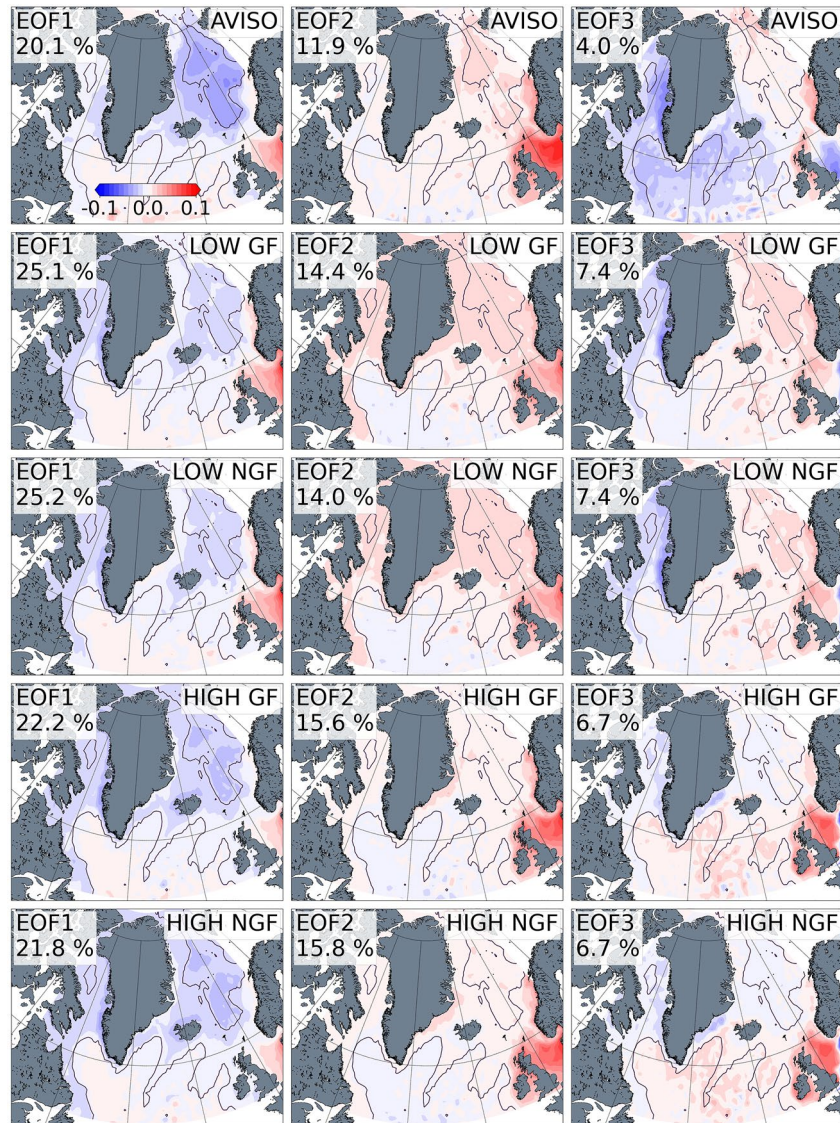
Figure 11. Map section for the first three leading EOFs including explained variance for AVISO and the four model simulations. The black contour lines represent bathymetry at 2,000 m depth.
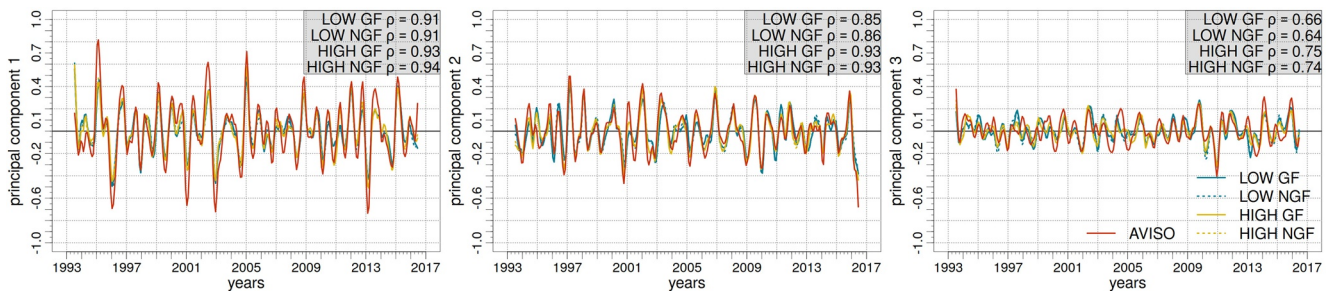

Figure 12. First three principal components of the simulations and AVISO, using the AVISO EOFs as the basis vector for the region shown in Figure 11. The correlations between AVISO and the model experiments are shown in the gray box.
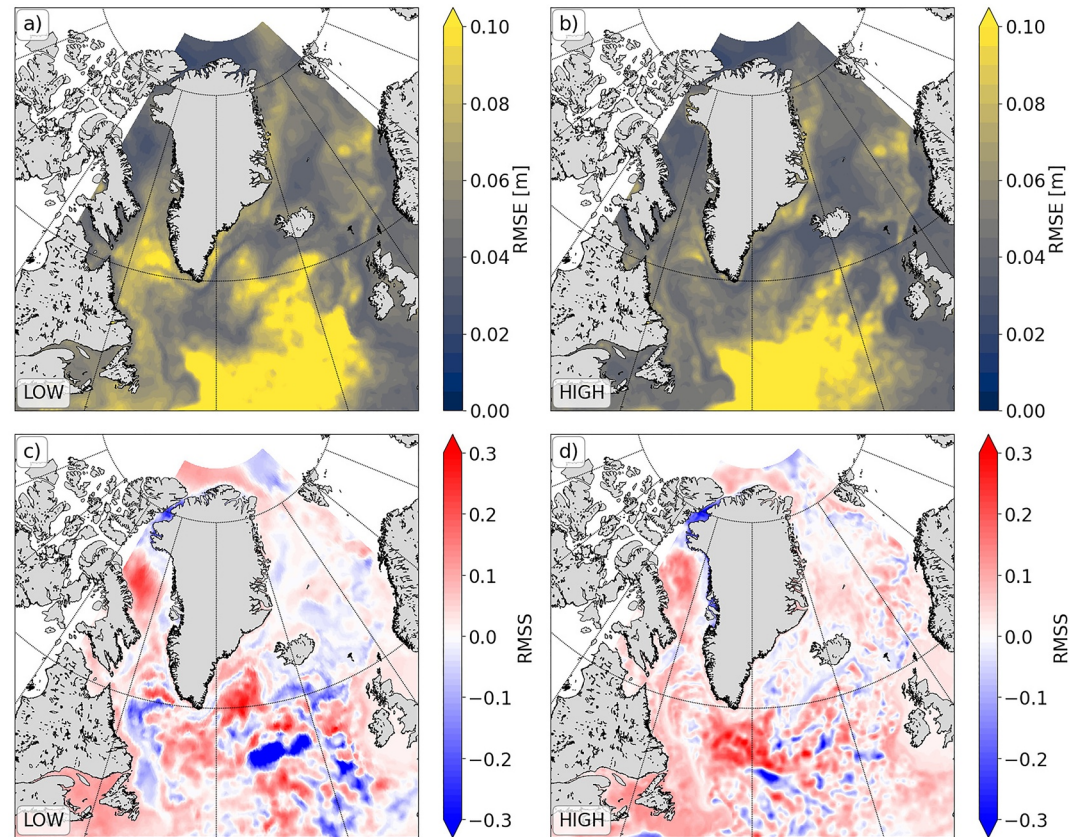
Figure 13. RMSE (in meter) for SLA for (a) LOW GF and (b) HIGH GF; Root mean square improvement (RMSS) for LOW GF with (c) LOW NGF as reference and respectively for (d) HIGH; Red shadings indicate an improvement of the GF-experiment compared to the NGF-experiment. White shadings indicate that the GF-experiment performs as good as the NGF-experiment. AVISO gridded sea level anomalies are used for comparison with model outputs. Mean and standard deviation (both regarding the areas of the pre-defined basins) of the RMSS for the predefined regions are shown in Table S6 of Supporting Information S1.

the ocean could be beneficial for a more realistic model representation regarding freshwater studies, for example, considering calving, where freshwater enters the ocean at deeper ocean layers (Straneo & Cenedese, 2015). Consequently, then the ice-sheet ocean interaction should be considered including physical-based calving criteria (Christmann et al., 2019). The impact of Greenland freshwater on the mixed layer depth is shown in Figure S4 of Supporting Information S1.

We investigate to what extent the melting signatures found in the model simulations are visible in different data sets, that is, altimetry, gravimetry, reanalysis data and Argo floats. This is not a detection-attribution study where one would have to simulate all possible competing forcing scenarios that could explain what is observed. Rather, we try to identify variables and regions where coherent differences can be found.

For Argo floats, we interpolate simulated model data to Argo float positions, which is new to our knowledge. In literature, it is common to use gridded data, such as the CORA reanalysis, where a variety of different observations, for example, from drifters, buoys, are included. The difficulty of using Argo only, however, is that Argo floats as well as other drifter types can be further transported by eddies. Eddies are not caused by atmospheric forcing but by baroclinic and barotropic instabilities. This means that such effects are not accounted for by forcing data but only in the model itself. Thus, it could lead to a representation problem in the model since eddies are not generated at the correct horizontal place. Moreover, as Argo floats are only available for around 10 years, this time period could be too small for these analyses. Although the analyzing time period of the Argo study is smaller than the time series comparisons with the ORAS5 reanalysis and CORA gridded data set, we find good agreement between the model simulations and the Argo data: in particular, the high-resolution model benefits from interpolating the simulations to the Argo positions. There are areas that are more sensitive to Greenland

melting rates, for example, the southeast of Greenland (area IS) close to the coast, with slight benefits compared to the reference run.

For the comparison with steric heights, the model agreements with other data sets show mixed results. We find that the Greenland melting effect is clearly visible in Baffin Bay and Davis Strait during the 1990s. In these regions Greenland freshwater accumulates over time (Figure S2a in Supporting Information S1 and Figures 4–5 in Bamber et al. [2018a]). The Greenland model experiments are in good agreement with ORAS5 and partly within its ensemble spread. For HIGH, we additionally find the area LS with slightly smaller RMSE values when including GF. We also use the inversion output, available since 2002, and determine that area IS and BB show clearly higher correlations and smaller errors (Tables S2–S5 in Supporting Information S1). The month-to-month signal of the simulation captures the phase well for the predefined regions with slight advantages for the Greenland experiments. The study by Chafik et al. (2019) indicates that in the subpolar gyre a positive trend between 1993 and 2004 and negative trend between 2005 and 2016 of steric heights is observed. Area ENA and IS cover parts of their study area. In IS, ORAS5 shows a strong increase until 2004/2005 and a weak decrease since then. For HIGH, the trend turning point (defined quantitatively) is 4 years earlier. The steric heights by Chafik et al. (2019) are based on the altimetry multi-mission data set including, amongst others, Envisat, SARAL/AltiKa, Jason which is used in the inversion method. Nevertheless, the negative trend of the inversion output is only visible since 2012/2013.

For sea level anomalies we find an improvement of up to 20% regarding the RMSE when including GF for both HIGH and LOW (see Figures 13c and 13d). This is clearly visible in Baffin Bay, the Labrador Sea (at least for HIGH), in the North Atlantic south of Greenland (improvement is more pronounced in HIGH) and in the Irminger Bay (at least for LOW). The correlations between the first two principal components of the model simulations and AVISO show large values (0.85 and larger). SLA from the high resolution model agrees better with AVISO regarding the correlations of the principal components, while the effect of Greenland meltwater is not visible in the EOF analysis.

Some areas around Greenland, notably the coastal zones and the west of Greenland, are seasonally covered with sea ice. In regions covered by sea ice, satellite altimeters can fail to identify the open water areas that must be sampled to measure sea surface height. Thus, the RMSE can be higher in these regions when comparing to other data or simulations when taking into account the seasons in which sea ice is present. However, there are missions that cope well with polar sea-ice covered areas, for example, Cryosat-2, which is part of the multi-mission product AVISO and thus fill or reduce some spatial gaps in the AVISO background ocean model. Another reason for discrepancies between simulated and observed sea level anomalies further south of Greenland, may be due to the model. Müller et al. (2019) listed and discussed possible weak points of FESOM in this context. One reason they assume is due to the relatively coarse resolution of the forcing data (55 km horizontal resolution) which could lead to a sea level smoothing. Furthermore, using sea level pressure as additional input variable could influence and improve simulated sea level anomalies.

Finally, we asked how sensitive ocean variables are with respect to model resolution. When comparing LOW and HIGH simulations with observations, we suggest that an increased model resolution can resolve small scale structures also in deeper ocean layers. This is evidenced by mostly higher correlation values and smaller errors, for example, for temperature and salinity. Wekerle, Wang, Danilov, et al. (2017) compared two model simulations performed with FESOM (24 and 4.5 km horizontal resolution in the Arctic Ocean) with the Arctic Regional Climatology and found that temperature and salinity is represented more realistically in the increased resolution setup with up to 50% improvement in RMSE for the Fram Strait. This fits to our comparisons for example, with Argo floats in region NSN, which includes Fram Strait, where we find lower RMSE values for HIGH compared to LOW. This improvement is also true for the other focus regions we have analyzed. The reasons for that are an improved mean circulation structure and eddies that are partially resolved or permitted in the higher resolution (Wekerle, Wang, Danilov, et al., 2017).

The effect of the increased model resolution is larger than the modeled melting effect for a large part of the time period and most areas. This could also be because the polygons based on bathymetry are too large and possible smaller freshwater signals are eliminated due to averaging effects. This study could therefore be the basis for further studies optimizing spatial fields in which the melting effect plays a greater role for essential climate variables such as for example, sea level anomalies. The ocean model, especially at high resolution, is sensitive to initial conditions and can lead to large differences in ocean properties due to emerging nonlinearities and

chaotic variability in the system (Sérazin et al., 2015). Ideally, an ensemble of simulations could help to test the robustness of the Greenland Ice Sheet fingerprints in light of different manifestations of turbulence in the ocean.

A weakness of this study is the applied surface salinity restoring. The sensitivity study by Behrens et al. (2013) shows that using no salinity restoring leads to a near collapse of the AMOC. Applying salinity restoring, however, leads to an artificial reduction of the Greenland runoff. We thus try to keep the salinity restoring as weak as possible while maintaining a realistic global ocean circulation. In most regions around Greenland, runoff exceeds the salinity restoring (Figure S2 in Supporting Information S1). There are some regions where relaxation dominates, for example, in Disko Bay and Scoresby Sund. The time series show that there are only a few months (especially in winter) when salinity restoring dominates the Greenland freshwater flux (Figure S1 in Supporting Information S1).

5. Summary

In this study, we investigated the effects of Greenland freshwater on ocean variables including salinity, temperature, steric heights and sea level anomalies. We find that improvements due to increased model resolution often dominates improvements from meltwater signatures in the ocean when comparing with observations, such as Argo floats, reanalysis data, altimetry and GRACE. The effects between the freshwater experiments are less distinctive when averaged over specific subdomains.

With our simulations and different types of observations, we show that Baffin Bay and Davis Strait are sensitive areas for Greenland melting signatures. Simulated steric height changes, obtained from the Greenland freshwater experiment, are in line with the ORAS5 ensemble especially in the 1990s and show an improvement of up to 36% in the mean absolute error when compared with the reference run that excludes Greenland freshwater. Modeled steric height changes in the Southeast (Irminger Sea) also improve with Greenland freshwater flux with an improvement of up to 27% for LOW (compared to the inversion output). The simulated impact of Greenland freshwater on temperature is up to 1°C and salinity up to −1 psu at the West coast of Greenland. This warming causes the temperature to rise above freezing by up to 1.6 months earlier in the year. Due to uncertainties in observations, simulations and spatial aggregations within the polygons, we find only small effects regarding the Greenland intrusion for temperature and salinity and other variables when evaluating these experiments.

Data Availability Statement

Model data and inversion output are available at https://doi.org/10.5281/zenodo.6243822.

References

Ackermann, L., Danek, C., Gierz, P., & Lohmann, G. (2020). AMOC recovery in a multicentennial scenario using a coupled atmosphere-ocean-ice sheet model. *Geophysical Research Letters*, *47*(16). https://doi.org/10.1029/2019GL086810

Argo. (2020). Argo float data and metadata from global data assembly centre [Dataset]. Argo GDAC. https://doi.org/10.17882/42182

Bamber, J., Tedstone, A. J., King, M. D., Howat, I. M., Enderlin, E. M., van den Broeke, M. R., & Noel, B. (2018a). Land ice freshwater budget of the Arctic and North Atlantic Oceans: 1. Data, methods, and results. *Journal of Geophysical Research: Oceans*, *123*(3), 1827–1837. https://doi.org/10.1002/2017JC013605

Bamber, J., Tedstone, A. J., King, M. D., Howat, I. M., Enderlin, E. M., van den Broeke, M. R., & Noel, B. (2018b). *Monthly modelled and observational freshwater flux time series for land ice in the Arctic and North Atlantic for 1958–2016*. British Oceanographic Data Centre, Natural Environment Research Council. https://doi.org/10.5285/643aa9bc-bcd6-45ad-e053-6c86abc07da0

Behrens, E., Biastoch, A., & Böning, C. W. (2013). Spurious AMOC trends in global ocean sea-ice models related to subarctic freshwater forcing. *Ocean Modelling*, *69*, 39–49. https://doi.org/10.1016/j.ocemod.2013.05.004

Brunnabend, S.-E., Schröter, J., Rietbroek, R., & Kusche, J. (2015). Regional sea level change in response to ice mass loss in Greenland, the West Antarctic and Alaska. *Journal of Geophysical Research: Oceans*, *120*(11), 7316–7328. https://doi.org/10.1002/2015JC011244

Böning, C. W., Behrens, E., Biastoch, A., Getzlaff, K., & Bamber, J. L. (2016). Emerging impact of Greenland meltwater on deepwater formation in the North Atlantic Ocean. *Nature Geoscience*, *9*(7), 523–527. https://doi.org/10.1038/ngeo2740

Böning, C., Timmermann, R., Macrander, A., & Schröter, J. (2008). A pattern-filtering method for the determination of ocean bottom pressure anomalies from GRACE solutions. *Geophysical Research Letters*, *35*(18), L18611. https://doi.org/10.1029/2008GL034974

Cabanes, C., Grouazel, A., von Schuckmann, K., Hamon, M., Turpin, V., Coatanoan, C., et al. (2013). The CORA dataset: Validation and diagnostics of in-situ ocean temperature and salinity measurements. *Ocean Science*, *9*(1), 1–18. https://doi.org/10.5194/os-9-1-2013

Carton, J. A., Penny, S. G., & Kalnay, E. (2019). Temperature and salinity variability in the SODA3, ECCO4r3, and ORAS5 ocean reanalyses, 1993–2015. *Journal of Climate*, *32*(8), 2277–2293. https://doi.org/10.1175/JCLI-D-18-0605.1

Castro de la Guardia, L., Hu, X., & Myers, P. G. (2015). Potential positive feedback between Greenland Ice Sheet melt and Baffin Bay heat content on the west Greenland shelf. *Geophysical Research Letters*, *42*(12), 4922–4930. https://doi.org/10.1002/2015GL064626

Chafik, L., Nilsen, J. E. Ø., Dangendorf, S., Reverdin, G., & Frederikse, T. (2019). North Atlantic Ocean circulation and decadal sea level change during the altimetry era. *Scientific Reports*, *9*, 1041. https://doi.org/10.1038/s41598-018-37603-6

Chelton, D. B., de Szoeke, R. A., Schlax, M. G., Naggar, K. E., & Siwertz, N. (1998). Geographical variability of the first baroclinic Rossby radius of deformation. *Journal of Physical Oceanography*, *28*(3), 433–460. https://doi.org/10.1175/1520-0485(1998)028<0433:gvotfb>2.0.co;2

Christmann, J., Müller, R., & Humbert, A. (2019). On nonlinear strain theory for a viscoelastic material model and its implications for calving of ice shelves. *Journal of Glaciology*, *65*(250), 212–224. https://doi.org/10.1017/jog.2018.107

Dahle, C., Flechtner, F., Gruber, C., König, D., König, R., Michalak, G., & Neumayer, K.-H. (2013). *GFZ GRACE level-2 processing standards document for level-2 product release 0005: Revised edition, January 2013, (scientific technical report STR - Data; 12/02 rev. ed.)* (p. 21). Deutsches GeoForschungsZentrum GFZ. https://doi.org/10.2312/GFZ.b103-1202-25

Danabasoglu, G., Yeager, S., Bailey, D., Behrens, E., Bentsen, M., Bi, D., et al. (2014). North Atlantic simulations in coordinated ocean-ice reference experiments phase II (CORE-II). Part I: Mean states. *Ocean Modelling*, *73*, 76–107. https://doi.org/10.1016/j.ocemod.2013.10.005

Danilov, S., Wang, Q., Timmermann, R., Iakovlev, N., Sidorenko, D., Kimmritz, M., et al. (2015). Finite-element sea ice model (FESIM), version 2. *Geoscientific Model Development*, *8*(6), 1747–1761. https://doi.org/10.5194/gmd-8-1747-2015

Devilliers, M., Swingedouw, D., Mignot, J., Deshayes, J., Garric, G., & Ayache, M. (2021). A realistic Greenland ice sheet and surrounding glaciers and ice caps melting in a coupled climate model. *Climate Dynamics*, *57*(9–10), 2467–2489. https://doi.org/10.1007/s00382-021-05816-7

Dukhovskoy, D. S., Myers, P. G., Platov, G., Timmermans, M.-L., Curry, B., Proshutinsky, A., et al. (2016). Greenland freshwater pathways in the sub-Arctic Seas from model experiments with passive tracers. *Journal of Geophysical Research: Oceans*, *121*(1), 877–907. https://doi.org/10.1002/2015JC011290

Dukhovskoy, D. S., Yashayaev, I., Proshutinsky, A., Bamber, J. L., Bashmachnikov, I. L., Chassignet, E. P., et al. (2019). Role of Greenland freshwater anomaly in the recent freshening of the subpolar North Atlantic. *Journal of Geophysical Research: Oceans*, *124*(5), 3333–3360. https://doi.org/10.1029/2018JC014686

Farrell, W. E., & Clark, J. A. (1976). On postglacial sea level. *Geophysical Journal International*, *46*(3), 647–667. https://doi.org/10.1111/j.1365-246X.1976.tb01252.x

Farrell, W. E., Cook, A. H., Jones, R. V., & King, G. C. P. (1973). A Discussion on the measurement and interpretation of changes of strain in the Earth - Earth tides, ocean tides and tidal loading. *Philosophical Transactions of the Royal Society of London - Series A: Mathematical and Physical Sciences*, *274*(1239), 253–259. https://doi.org/10.1098/rsta.1973.0050

Fox-Kemper, B., Hewitt, H., Xiao, C., Aðalgeirsdóttir, G., Drijfhout, S., Edwards, T., et al. (2021). Ocean, cryosphere and sea level change. In V. Masson-Delmotte, P. Zhai, A. Pirani, S. L. Connors, C. Péan, S. Berger, et al. (Eds.), *Climate Change 2021: The Physical Science Basis. Contribution of Working Group 1 to the Sixth Assessment Report of the Intergovernmental Panel on Climate Change* (pp. 1211–1362). Cambridge University Press. https://doi.org/10.1017/9781009157896.011

Gerdes, R., Hurlin, W., & Griffies, S. M. (2006). Sensitivity of a global ocean model to increased run-off from Greenland. *Ocean Modelling*, *12*(3–4), 416–435. https://doi.org/10.1016/j.ocemod.2005.08.003

Gillard, L., Hu, X., Myers, P., & Bamber, J. (2016). Meltwater pathways from marine terminating glaciers of the Greenland ice sheet. *Geophysical Research Letters*, *43*(20), 10873–10882. https://doi.org/10.1002/2016GL070969

Glowienka-Hense, R., Hense, A., Brune, S., & Baehr, J. (2020). Comparing forecast systems with multiple correlation decomposition based on partial correlation. *Advances in Statistical Climatology, Meteorology and Oceanography*, *6*(2), 103–113. https://doi.org/10.5194/ascmo-6-103-2020

Greatbatch, R. J. (1994). A note on the representation of steric sea level in models that conserve volume rather than mass. *Journal of Geophysical Research*, *99*(C6), 12767–12771. https://doi.org/10.1029/94JC00847

Hallberg, R. (2013). Using a resolution function to regulate parameterizations of oceanic mesoscale eddy effects. *Ocean Modelling*, *72*, 92–103. https://doi.org/10.1016/j.ocemod.2013.08.007

Holliday, N. P., Bersch, M., Berx, B., Chafik, L., Cunningham, S., Florindo-López, C., et al. (2020). Ocean circulation causes the largest freshening event for 120 years in eastern subpolar North Atlantic. *Nature Communications*, *11*(585), 585. https://doi.org/10.1038/s41467-020-14474-y

Hoteit, I., Luo, X., Bocquet, M., Köhl, A., & Ait-El-Fquih, B. (2018). Data assimilation in oceanography: Current status and new directions. In (pp. 465–511). https://doi.org/10.17125/gov2018.ch17

Hunke, E. C., & Dukowicz, J. K. (1997). An elastic–viscous–plastic model for sea ice dynamics. *Journal of Physical Oceanography*, *27*(9), 1849–1867. https://doi.org/10.1175/1520-0485(1997)027<1849:aevpmf>2.0.co;2

Kienert, H., & Rahmstorf, S. (2012). On the relation between meridional overturning circulation and sea-level gradients in the Atlantic. *Earth System Dynamics*, *3*(2), 109–120. https://doi.org/10.5194/esd-3-109-2012

Kleinen, T., Osborn, T. J., & Briffa, K. R. (2009). Sensitivity of climate response to variations in freshwater hosing location. *Ocean Dynamics*, *59*(3), 509–521. https://doi.org/10.1007/s10236-009-0189-2

Kobayashi, S., Ota, Y., Harada, Y., Ebita, A., Moriya, M., Onoda, H., et al. (2015). The JRA-55 reanalysis: General specifications and basic characteristics. *Journal of the Meteorological Society of Japan. Series II*, *93*(1), 5–48. https://doi.org/10.2151/jmsj.2015-001

Kuhlmann, J., Dobslaw, H., & Thomas, M. (2011). Improved modeling of sea level patterns by incorporating self-attraction and loading. *Journal of Geophysical Research*, *116*(C11), C11036. https://doi.org/10.1029/2011JC007399

Kvas, A., Behzadpour, S., Ellmer, M., Klinger, B., Strasser, S., Zehentner, N., & Mayer-Gürr, T. (2019). ITSG-Grace2018: Overview and evaluation of a new GRACE-only gravity field time series. *Journal of Geophysical Research: Solid Earth*, *124*(8), 9332–9344. https://doi.org/10.1029/2019JB017415

Marson, J. M., Gillard, L. C., & Myers, P. G. (2021). Distinct ocean responses to Greenland's liquid runoff and iceberg melt. *Journal of Geophysical Research: Oceans*, *126*(12), e2021JC017542. https://doi.org/10.1029/2021JC017542

Mayer-Gürr, T., Behzadpour, S., Ellmer, M., Kvas, A., Klinger, B., Strasser, S., & Zehentner, N. (2018). *ITSG-Grace2018 - Monthly, daily and static gravity field solutions from GRACE*. GFZ Data Services. https://doi.org/10.5880/ICGEM.2018.003

McDougall, T. J., & Barker, P. M. (2011). Getting started with TEOS-10 and the Gibbs Seawater (GSW) Oceanographic Toolbox, SCOR/IAPSO WG127 (p. 28), ISBN 978-0-646-55621-5.

Mouginot, J., Rignot, E., Bjørk, A. A., van den Broeke, M., Millan, R., Morlighem, M., et al. (2019). Forty-six years of Greenland Ice Sheet mass balance from 1972 to 2018. *Proceedings of the National Academy of Sciences*, *116*(19), 9239–9244. https://doi.org/10.1073/pnas.1904242116

Müller, F. L., Wekerle, C., Dettmering, D., Passaro, M., Bosch, W., & Seitz, F. (2019). Dynamic ocean topography of the northern Nordic seas: A comparison between satellite altimetry and ocean modeling. *The Cryosphere*, *13*(2), 611–626. https://doi.org/10.5194/tc-13-611-2019

Owens, W. B., & Lemke, P. (1990). Sensitivity studies with a sea ice-mixed layer-pycnocline model in the Weddell Sea. *Journal of Geophysical Research*, *95*(C6), 9527–9538. https://doi.org/10.1029/JC095iC06p09527

Parkinson, C. L., & Washington, W. M. (1979). A large-scale numerical model of sea ice. *Journal of Geophysical Research*, *84*(C1), 311–337. https://doi.org/10.1029/JC084iC01p00311

Proshutinsky, A., Steele, M., & Timmermans, M.-L. (2016). Forum for Arctic modeling and observational synthesis (FAMOS): Past, current, and future activities. *Journal of Geophysical Research: Oceans*, *121*(6), 3803–3819. https://doi.org/10.1002/2016JC011898

Richter, M. E., von Appen, W.-J., & Wekerle, C. (2018). Does the East Greenland current exist in the northern Fram Strait? *Ocean Science*, *14*(5), 1147–1165. https://doi.org/10.5194/os-14-1147-2018

Rietbroek, R., Brunnabend, S.-E., Kusche, J., Schröter, J., & Dahle, C. (2016). Revisiting the contemporary sea-level budget on global and regional scales. *Proceedings of the National Academy of Sciences*, *113*(6), 1504–1509. https://doi.org/10.1073/pnas.1519132113

Sasgen, I., Wouters, B., Gardner, A., King, M., Tedesco, M., Landerer, F., et al. (2020). Return to rapid ice loss in Greenland and record loss in 2019 detected by the GRACE-FO satellites. *Communication Earth & Environment*, *1*, 8. https://doi.org/10.1038/s43247-020-0010-1

Schaffer, J., Timmermann, R., Arndt, J. E., Kristensen, S. S., Mayer, C., Morlighem, M., & Steinhage, D. (2016). A global, high-resolution data set of ice sheet topography, cavity geometry, and ocean bathymetry. *Earth System Science Data*, *8*(2), 543–557. https://doi.org/10.5194/essd-8-543-2016

Scharroo, R., Leuliette, E. W., Lillibridge, J. L., Byrne, D., Naeije, M. C., & Mitchum, G. T. (2013). RADS: Consistent multi-mission products. In *Proceedings of the symposium on 20 Years of progress in radar altimetry, Venice, 20–28 September 2012. European Space Agency Special Publication, ESA SP-710* (p. 4).

Scholz, P., Kieke, D., Lohmann, G., Ionita, M., & Rhein, M. (2014). Evaluation of Labrador Sea Water formation in a global Finite-Element Sea-Ice Ocean Model setup, based on a comparison with observational data. *Journal of Geophysical Research: Oceans*, *119*(3), 1644–1667. https://doi.org/10.1002/2013JC009232

Seidov, D., Antonov, J., Arzayus, K., Baranova, O., Biddle, M., Boyer, T., et al. (2015). Oceanography north of 60°N from World Ocean database. *Progress in Oceanography*, *132*, 153–173. https://doi.org/10.1016/j.pocean.2014.02.003

Sein, D. V., Koldunov, N. V., Danilov, S., Wang, Q., Sidorenko, D., Fast, I., et al. (2017). Ocean modeling on a mesh with resolution following the local Rossby radius. *Journal of Advances in Modeling Earth Systems*, *9*(7), 2601–2614. https://doi.org/10.1002/2017MS001099

Sidorenko, D., Danilov, S., Fofonova, V., Cabos, W., Koldunov, N., Scholz, P., et al. (2020). AMOC, water mass transformations, and their responses to changing resolution in the Finite-volumE Sea ice-Ocean model. *Journal of Advances in Modeling Earth Systems*, *12*(12), e2020MS002317. https://doi.org/10.1029/2020MS002317

Stammer, D. (2008). Response of the global ocean to Greenland and Antarctic ice melting. *Journal of Geophysical Research*, *113*(C6), C06022. https://doi.org/10.1029/2006JC004079

Stammer, D., Balmaseda, M., Heimbach, P., Köhl, A., & Weaver, A. (2016). Ocean data assimilation in support of climate applications: Status and perspectives. *Annual Review of Marine Science*, *8*(1), 491–518. https://doi.org/10.1146/annurev-marine-122414-034113

Steele, M., Morley, R., & Ermold, W. (2001). PHC: A global ocean hydrography with a high-quality Arctic Ocean. *Journal of Climate*, *14*(9), 2079–2087. https://doi.org/10.1175/1520-0442(2001)014<2079:pagohw>2.0.co;2

Stolzenberger, S., Glowienka-Hense, R., Spangehl, T., Schröder, M., Mazurkiewicz, A., & Hense, A. (2015). Revealing skill of the MiKlip decadal prediction systems by three-dimensional probabilistic evaluation. *Meteorologische Zeitschrift*, *25*(6), 657–671. https://doi.org/10.1127/metz/2015/0606

Straneo, F., & Cenedese, C. (2015). The dynamics of Greenland's glacial fjords and their role in climate. *Annual Review of Marine Science*, *7*(1), 89–112. https://doi.org/10.1146/annurev-marine-010213-135133

Swingedouw, D., Rodehacke, C. B., Behrens, E., Menary, M., Olsen, S. M., Gao, Y., et al. (2013). Decadal fingerprints of freshwater discharge around Greenland in a multi-model ensemble. *Climate Dynamics*, *41*(3–4), 695–720. https://doi.org/10.1007/s00382-012-1479-9

Szekely, T., Gourrion, J., Pouliquen, S., & Reverdin, G. (2019). CORA, Coriolis Ocean dataset for ReAnalysis [Dataset]. SEANOE. https://doi.org/10.17882/46219

Sérazin, G., Penduff, T., Grégorio, S., Barnier, B., Molines, J.-M., & Terray, L. (2015). Intrinsic variability of sea level from global ocean simulations: Spatiotemporal scales. *Journal of Climate*, *28*(10), 4279–4292. https://doi.org/10.1175/JCLI-D-14-00554.1

Tesdal, J.-E., Abernathey, R., Goes, J., Gordon, A., & Haine, T. (2018). Salinity trends within the upper layers of the subpolar North Atlantic. *Journal of Climate*, *31*(7), 2675–2698. https://doi.org/10.1175/JCLI-D-17-0532.1

The IMBIE Team, Shepherd, A., Ivins, E., Rignot, E., Smith, B., van den Broeke, M., et al. (2020). Mass balance of the Greenland Ice Sheet from 1992 to 2018. *Nature*, *579*(7798), 233–239. https://doi.org/10.1038/s41586-019-1855-2

Timmermann, R., Danilov, S., Schröter, J., Böning, C., Sidorenko, D., & Rollenhagen, K. (2009). Ocean circulation and sea ice distribution in a finite element global sea ice–ocean model. *Ocean Modelling*, *27*(3), 114–129. https://doi.org/10.1016/j.ocemod.2008.10.009

Uebbing, B., Kusche, J., Rietbroek, R., & Landerer, F. W. (2019). Processing choices affect ocean mass estimates from GRACE. *Journal of Geophysical Research: Oceans*, *124*(2), 1029–1044. https://doi.org/10.1029/2018JC014341

Wang, Q., Danilov, S., Sidorenko, D., Timmermann, R., Wekerle, C., Wang, X., et al. (2014). The Finite Element Sea Ice-Ocean Model (FESOM) v. 1.4: Formulation of an ocean general circulation model. *Geoscientific Model Development*, *7*(2), 663–693. https://doi.org/10.5194/gmd-7-663-2014

Wang, Q., Wekerle, C., Danilov, S., Wang, X., & Jung, T. (2018). A 4.5 km resolution Arctic Ocean simulation with the global multi-resolution model FESOM 1.4. *Geoscientific Model Development*, *11*(4), 1229–1255. https://doi.org/10.5194/gmd-11-1229-2018

Wang, Q., Wekerle, C., Wang, X., Danilov, S., Koldunov, N., Sein, D., et al. (2020). Intensification of the Atlantic water supply to the Arctic Ocean through Fram Strait induced by Arctic sea ice decline. *Geophysical Research Letters*, *47*(3), e2019GL086682. https://doi.org/10.1029/2019GL086682

Wang, X., Wang, Q., Sidorenko, D., Danilov, S., Schröter, J., & Jung, T. (2012). Long-term ocean simulations in FESOM: Evaluation and application in studying the impact of Greenland Ice Sheet melting. *Ocean Dynamics*, *62*(10–12), 1471–1486. https://doi.org/10.1007/s10236-012-0572-2

Wekerle, C., Wang, Q., Danilov, S., Schourup-Kristensen, V., von Appen, W.-J., & Jung, T. (2017). Atlantic Water in the Nordic Seas: Locally eddy-permitting ocean simulation in a global setup. *Journal of Geophysical Research: Oceans*, *122*(2), 914–940. https://doi.org/10.1002/2016JC012121

Wekerle, C., Wang, Q., von Appen, W.-J., Danilov, S., Schourup-Kristensen, V., & Jung, T. (2017). Eddy-resolving simulation of the Atlantic water circulation in the Fram Strait with focus on the seasonal cycle. *Journal of Geophysical Research: Oceans*, *122*(11), 8385–8405. https://doi.org/10.1002/2017JC012974

Zuo, H., Balmaseda, M. A., Tietsche, S., Mogensen, K., & Mayer, M. (2019). The ECMWF operational ensemble reanalysis–analysis system for ocean and sea ice: A description of the system and assessment. *Ocean Science*, *15*(3), 779–808. https://doi.org/10.5194/os-15-779-2019

Zuo, H., Balmaseda, M., & Mogensen, K. (2017). The new eddy-permitting ORAP5 ocean reanalysis: Description, evaluation and uncertainties in climate signals. *Climate Dynamics*, *49*(3), 791–811. https://doi.org/10.1007/s00382-015-2675-1